OPEN-CIRCUIT SELF-DISCHARGE BEHAVIOR OF NICKEL-HYDROGEN BATTERIES

Thesis

Submitted to

Graduate Engineering & Research
School of Engineering

UNIVERSITY OF DAYTON

In Partial Fulfillment of the Requirements for

The Degree

Master of Science in Chemical Engineering

by

Joseph P. Fellner

UNIVERSITY OF DAYTON

Dayton, Ohio

July 1991

OPEN-CIRCUIT SELF-DISCHARGE BEHAVIOR NICKEL-HYDROGEN BATTERIES

APPROVED BY

Sarwan S. Sandhu, Ph.D.
Advisory Committee, Chairman

Gary A. Thiele, Ph.D.
Associate Dean/Director
Graduate Engineering & Research
School of Enigneering

Patrick J. Sweeney, Ph.D.
Dean, School of Enigneering

ABSTRACT

OPEN CIRCUIT SELF-DISCHARGE BEHAVIOR OF NICKEL-HYDROGEN BATTERIES

Name: Fellner, Joseph Phillip
University of Dayton, 1991

Advisor: Dr. S. S. Sandhu

Nickel-hydrogen batteries are a proven technology for space satellites with a long cycle life, high energy and power density, true state-of-charge indication, and excellent over-charge and cell reversal protection. Further use of this battery technology would be enhanced by the reduction in the battery self-discharge rate on open-circuit. In order to develop ways to reduce this self-discharge rate, a fundamental understanding of the self-discharge processes is vital.

The purpose of the research was to investigate the mechanism(s) for the self-discharge of nickel-hydrogen batteries on open-circuit. A detailed mass transfer and reaction model was developed to characterize the transfer and reaction of the hydrogen gas. Open-circuit measurements of the hydrogen pressure with time of a 54.7 amp-hour nickel-hydrogen cell were used to verify the model.

The results of this investigation are that the open-circuit hydrogen pressure of a initially fully charged nickel-hydrogen cell decays in accord with a high Thiele Modulus, diffusion-limited reaction. By decreasing the amount of charge prior to open-circuit, the

hydrogen pressure decay rate decreases in accord with a decreased Thiele Modulus. Therefore, the open-circuit self-discharge rate is not a solely kinetic-limited reaction as previously proposed in the literature.

TABLE OF CONTENTS

LIST OF FIGURES

LIST OF SYMBOLS

a_{H_2O}	activity of water
a_{KOH}	activity of potassium hydroxide
A	amp-hour capacity
A_o	initial amp-hour capacity
C_1	hydrogen concentration
C_2	β-NiOOH concentration
$C_{1,o}$	initial hydrogen gas concentration
$C_{1,p}$	precharge hydrogen gas concentration
$C_{1,s}$	hydrogen concentration at the electrolyte/nickel active material interface
$C_{2,o}$	initial β-NiOOH concentration
D_e	effective diffusivity
H	Henry's Law constant
k_1	first order rate constant
k_2	second order rate constant
L_a	thickness of active material
M^2	$R_1(C_{1,s};C_{2,o})/(D_eC_{1,s}/L_a^2)$; the Thiele Modulus squared which is indicative of the ratio of the maximum reaction rate over a characteristic diffusion rate

n_1	moles of hydrogen
N_1	hydrogen flux rate
n_2	moles of β-NiOOH
P_1	absolute hydrogen pressure corrected for compressibility
$P_{1,o}$	initial corrected hydrogen pressure
$P_{1,p}$	precharge corrected hydrogen pressure
R_1	rate of hydrogen consumption
R_1^*	$R_1/R_1(C_{1,s};C_{2,o})$; dimensionless hydrogen consumption rate
R_2	rate of β-NiOOH consumption
S	electrolyte/nickel active material interfacial area
t	time
t*	$D_e/\varepsilon L_a^2$; dimensionless time
x	distance in nickel active material
xf	distance in nickel active material where diffusion-limited reaction front occurs
X_2	fractional conversion of β-NiOOH
V_b	battery gas volume

GREEK LETTERS

ε	β-$Ni(OH)_2$ porosity
ϕ_1	$C_1/C_{1,s}$; dimensionless hydrogen concentration
ϕ_2	$C_2/C_{2,o}$; dimensionless β-NiOOH concentration
ξ	x/L_a; dimensionless distance

ρ_2	β-NiOOH molar density
τ	$2R_1(C_{1,s};C_{2,o})t/C_{2,o}$; dimensionless time

LIST OF SPECIAL NOMENCLATURE

active material	the material within the electrodes that is electrochemically active and contributes to cell capacity
amp-hour	3600 coulombs
battery	an electrochemical storage device consisting of a number of cells
"C/n" rate	the constant current charge/discharge rate where "n" hours are required to fully charge or discharge the battery based on the battery's theoretical capacity
cell	an electrochemical storage device consisting of a single anode/cathode pair with supporting electrolyte
cell anode	cell electrode where the oxidation reaction occurs on discharge
cell cathode	cell electrode where the reduction reaction occurs on discharge
cell reversal	condition where a cell in the battery is forced to operate at less than 0 volts potential difference as measured between the cell cathode and cell anode
cell voltage roll-over	occurrence on charging of a battery with constant current where the battery voltage stops increasing and starts to decrease signifying end of charge and the start of over-charging
charge efficiency	the amount of current that electrochemically charges the battery divided by the total charge current
corrected pressure	absolute battery pressure divided by the compressibility factor and the gas absolute temperature and multiplied by 298.15K
current collector	electron conducting material used to distribute electronic current

cycle life	number of useable battery charge/discharge cycles
electrolyte-starved	this term is used to signify that only a given portion of the electrode pore volume is filled with electrolyte
energy density	energy delivered by battery on discharge divided by battery weight
flooded-electrolyte	this term is used to signify that all of the pores within the electrode are filled with electrolyte
macropores	electrode active material pores with radii greater than 1000 Å.
micropores	electrode active material pores with radii less than 1000 Å.
negative electrode	the electrode in a cell in which the oxidation reaction occurs on discharge
open-circuit	a battery that is not being electrically charged or discharged
over-charge	for the Ni-H_2 battery used here, this is charging a battery past cell voltage roll-over
positive electrode	the electrode in a cell in which the reduction reaction occurs on discharge
power density	power delivered by battery on discharge divided by battery weight
self-discharge	the parasitic loss of a cell's coulombic capacity by various mechanisms
state-of-charge indication	reading from the battery based on some battery parameter on the amount of charge available from the battery relative to full charge

CHAPTER I

INTRODUCTION

The nickel-hydrogen (Ni-H_2) battery is really a hybrid battery/fuel cell. The technology for the nickel-hydrogen battery was derived from the nickel-cadmium (Ni-Cd) battery's nickel electrode and the hydrogen-oxgyen fuel cell's hydrogen electrode. Some operational benefits gained by the marriage of these two couples are long cycle life, high energy and power density, excellent over-charge and cell reversal protection and a true state-of-charge indication. One of its major drawbacks, however, is a relatively high self-discharge rate. At 20°C and an internal hydrogen gas storage pressure of 30 to 50 bars, a typical Ni-H_2 battery may be expected to lose up to 50% of its electrochemical capacity in 8 days.[1]

The main cell reactions occuring in the Ni-H_2 battery at the positive and negative electrodes are shown, respectively, below.[2]

$$2\beta\text{-}NiOOH_{(s)} + 2H_2O_{(l)} + 2e^- \rightleftharpoons 2\beta\text{-}Ni(OH)_{2(s)} + 2OH^-_{(l)} \qquad (1.1)$$

$$H_{2(g)} + 2OH^-_{(l)} \rightleftharpoons 2H_2O_{(l)} + 2e^- \qquad (1.2)$$

The overall cell reaction is

$$H_{2(g)} + 2\beta\text{-}NiOOH_{(s)} \rightleftharpoons 2\beta\text{-}Ni(OH)_{2(s)} \qquad (1.3)$$

Thus, hydrogen gas is consumed on discharge and produced on charge. The pressure of hydrogen is, therefore, an accurate indication of the capacity of the battery at any given time.

When charging nears completion, the charging efficiency of the nickel electrode decreases and oxygen will start to evolve at the nickel electrode.[3] The oxygen evolution half-cell reaction can be simplified as occuring by

$$4OH^-_{(l)} \rightleftharpoons O_{2_{(g)}} + 2H_2O_{(l)} + 4e^- \qquad (1.4)$$

Oxygen may also evolve on open-circuit at the nickel electrode at elevated temperatures by self-discharge with the β-NiOOH as shown below.

$$2\beta\text{-}NiOOH_{(s)} + H_2O_{(l)} \rightleftharpoons 2\beta\text{-}Ni(OH)_{2(s)} + \frac{1}{2}O_{2(g)} \qquad (1.5)$$

By the use of additives such as lithium and cobalt hydroxides, measured oxygen gas concentrations in Ni-H_2 batteries after being charged are typically 0.1% by volume or less.[4]

The open-circuit self-discharge rate of Ni-H_2 batteries, however, is much higher than other nickel type batteries such as nickel-cadmium in which the self-discharge is due only to oxygen evolution.[1] The hydrogen, in the Ni-H_2 battery, reacts directly with the nickel electrode active material as shown below.[5]

$$H_{2(g)} + 2\beta\text{-}NiOOH_{(s)} \rightarrow 2\beta\text{-}Ni(OH)_{2(s)} \qquad (1.6)$$

A literature search for postulated self-discharge reaction mechanisms was conducted. A mathematical model based on diffusion and kinetics was developed to further describe

the self-discharge mechanism. Mathematical models obtained from the literature search and the model developed under this effort were compared and contrasted with experimental data. The model developed under this effort is more consistent with the experimental data and explains in greater detail the phenomenon occuring during self-discharge of the Ni-H_2 battery.

CHAPTER II

LITERATURE REVIEW

A literature search was conducted to determine the reaction mechanism(s) for the self-discharge of Ni-H_2 batteries. In order to establish a sound basis for the reaction mechanism(s), the search was performed on the Ni-H_2 electrochemical thermodynamics and cell self-discharge reaction kinetics.

Ni-H_2 Electrochemical Thermodynamics

The main cell reactions that occur in the Ni-H_2 battery are best represented by

$$2\beta\text{-}NiOOH_{(s)} + 2H_2O_{(l)} + 2e^- \rightleftharpoons 2\beta\text{-}Ni(OH)_{2(s)} + 2OH^-_{(l)} \qquad (2.1)$$

$$H_{2(g)} + 2OH^-_{(l)} \rightleftharpoons 2H_2O_{(l)} + 2e^- \qquad (2.2)$$

with the overall cell reaction being

$$H_{2(g)} + 2\beta\text{-}NiOOH_{(s)} \rightleftharpoons 2\beta\text{-}Ni(OH)_{2(s)} \qquad (2.3)$$

The structure of well crystallized β-$Ni(OH)_2$, based on X-ray and neutron diffraction results, is of the brucite C6-type structure with unit cell dimensions of a_o = 3.126 Å and c_o = 4.605 Å and is isomorphous with the divalent hydroxides of Ca, Mg, Fe, Co, and Cd.[2,6] Well crystallized β-$Ni(OH)_2$ is electrochemically inactive in contrast to the

hydrated, high surface area β-$Ni(OH)_2$ used in batteries. Structural determinations for the electrochemically active material used in batteries are complicated because of the amorphous nature. However, cell dimensions for hydrated, high surface area β-$Ni(OH)_2$ are reported to be a_o = 3.119 Å and c_o = 4.686 Å.

The β-NiOOH used in batteries is also amorphous in crystal structure. However, it is reported to be of relatively the same brucite structure as the β-$Ni(OH)_2$ with cell dimensions of a_o = 2.82 Å and c_o = 4.85 Å.

On extended overcharge, the β-NiOOH may be converted to γ-NiOOH.[2] The γ-NiOOH on discharge converts to α-$Ni(OH)_2$. During normal battery operation, γ-NiOOH is not formed. Thus, the formation of and subsequent reaction of hydrogen with γ-NiOOH and α-$Ni(OH)_2$ will not be considered.

The reversible open-circuit potential of the hydrogen reaction, Eq. (2.2), is easily calculated by standard thermodynamic techniques. However, the reversible open-circuit potential of the β-NiOOH reduction reaction, Eq. (2.1), is not easy to obtain since it self-discharges by the reaction shown in Eq. (1.4) and, in the presence of hydrogen gas, Eq. (1.6). Barnard, et.al used the method of Conway and Borgault to determine the reversible potentials of the β-NiOOH reduction reaction.[7] Their equation for the reversible potential of reaction, Eq. (2.1), with respect to the normal hydrogen electrode, is given below.

$$E_r = 1.3688 - 0.0028\log(a_{KOH}) + 0.0315\log(a_{H_2O}) \qquad (2.4)$$

For low hydrogen pressures, the reversible open-circuit potential of reaction given by Eq. (2.3) then can be represented by

$$E^o_{cell} = 1.3688 - 0.0028\log(a_{KOH}) + 0.0315\log(a_{H_2O}) + 0.0296\log(P_1) \qquad (2.5)$$

Thus, the reversible cell voltage will go up with decreasing potassium hydroxide concentration and increasing cell hydrogen pressure.

The chemical reaction of β-NiOOH with H_2 is calculated to yield 144,851 Joules/gram-mole of β-NiOOH.[8] The chemical reaction of β-$Ni(OH)_2$ with hydrogen is calculated to yield 32,586 Joules/gram-mole of β-$Ni(OH)_2$. However, the chemical reaction of β-$Ni(OH)_2$ with hydrogen to form nickel metal and water occurs at such a slow rate that this reaction will not be considered in the analysis.[5]

Cell Self-Discharge Reaction Kinetics

Historically, the rate of self-discharge of nickel-hydrogen batteries has been proposed to be of kinetic control and to be of first order with respect to hydrogen concentration.[9-11] For constant temperature and battery volume, the equation for battery pressure with time would then be expressed by the equation shown below.

$$\ln(P_t) = \ln(P_{t,o}) - k_1 t \tag{2.6}$$

However, this first order relation appears to conflict with calorimetric data performed at constant hydrogen pressure where the self-discharge rate is not constant with time as would be predicted from first order kinetics.[5,12-14] The heat generation rate (h) can be fitted to the relation:

$$h = \frac{a}{\sqrt{t}} \tag{2.7}$$

Thus, the self-discharge reaction fits the form of a diffusion-limited reaction and is not under first order kinetic control.

The rate of self-discharge of nickel-hydrogen batteries has also been proposed to be proportional to the concentration of hydrogen and the state of charge of the nickel electrode.[15] This rate equation is shown below.

$$-\frac{1}{V_b}\frac{dn_1}{dt} = k_2 C_1 C_2 \tag{2.8}$$

Nickel-hydrogen batteries typically operate with excess hydrogen or a "pre-charge" which is the amount of hydrogen that is used to fill the fully discharged battery initially. Thus, the capacity of the nickel electrode is proportional to the difference in the hydrogen battery pressure and the precharge pressure. With this, the fraction of unconverted β-NiOOH can be defined as:

$$C_2 = C_{2,o}(1-X_2) = C_{2,o}\left(\frac{C_1 - C_{1,p}}{C_{1,o} - C_{1,p}}\right) \tag{2.9}$$

Assuming constant temperature and using Eqs. (2.8) and (2.9), the battery pressure as a function of open-circuit time for this second order kinetic case is shown below.

$$\ln\left(\frac{P_1}{P_1 - P_{1,p}}\right) = \frac{k_2(P_{1,p})(C_{2,o})}{(P_{1,o} - P_{1,p})}t + \ln\left(\frac{P_{1,o}}{P_{1,o} - P_{1,p}}\right) \tag{2.10}$$

This second order rate expression, like the first order rate expression, ignores the effects of mass transfer. Mao, et. al.,[13] found that the self-discharge rate was greatly influenced by the degree of immersion of the nickel electrode with electrolyte. This implies that for "flooded-electrolyte" Ni-H_2 batteries, the diffusion of hydrogen within the electrolyte may greatly reduce the rate of self-discharge as compared to "less-flooded electrolyte" or "electrolyte-starved" batteries.

Discussion of kinetics versus hydrogen diffusion within the electrolyte is further given by Zhang, et. al.[14]

CHAPTER III

SELF-DISCHARGE MODEL

To promote rapid oxygen recombination on overcharge, the nickel electrode of the nickel-hydrogen battery operates in an "electrolyte-starved" condition.[4,16] Therefore, the electrolyte is only present in the micropores of the active material and the macropores of the nickel electrode are free of electrolyte for rapid transport of oxygen produced on overcharge. Assuming that the nickel active material/electrolyte is a homogeneous mixture, the nickel electrode can be modeled as shown in Fig. 1. Due to low mass transfer rates, psuedo steady-state thermodynamic equilibrium is assumed for hydrogen at the interface (x=0) and the concentration of the dissolved gas at the interface can be represented by Henry's Law. This hydrogen that is dissolved in the electrolyte and transported in the homogeneous active material/electrolyte mixture, chemically reacts with β-NiOOH to β-$Ni(OH)_2$ as given by Eq. (1.6). A one dimensional mass balance on hydrogen at x=x, (Fig. 1), assuming constant density, porosity and diffusivity, and no convection results in

$$\varepsilon \frac{\partial C_1}{\partial t} = D_e \frac{\partial^2 C_1}{\partial x^2} - R_1 \tag{3.1}$$

A mass balance on the nickel oxyhydroxide yields

$$\frac{\partial C_2}{\partial t} = -R_2 = -2R_1 \tag{3.2}$$

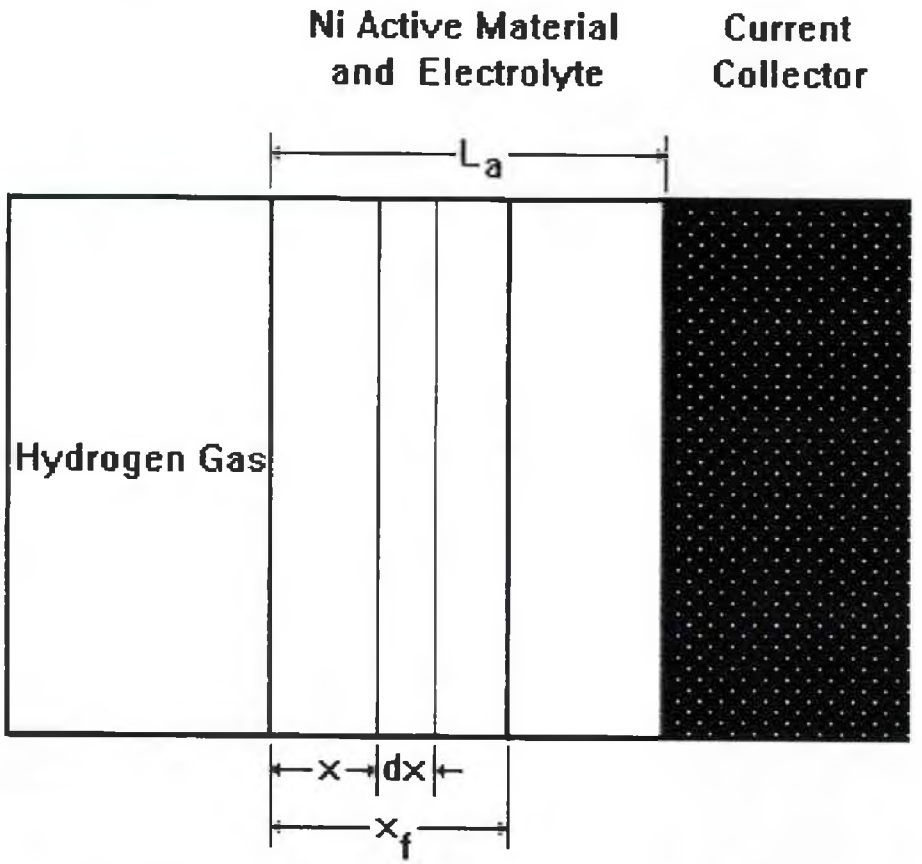

Figure 1. Schematic Diagram of Nickel Electrode.

In dimensionless form, Eqs. (3.1) and (3.2) become

$$\left(\frac{2C_{1,s}\varepsilon}{C_{2,o}}\right)\frac{\partial\phi_1}{\partial\tau} = \frac{1}{M^2}\frac{\partial^2\phi_1}{\partial\xi^2} - R_1^* \tag{3.3}$$

$$\frac{\partial\phi_2}{\partial\tau} = -R_1^* \tag{3.4}$$

When the term defined by M^2 is small, ($M^2<<1$), the hydrogen diffusion rate is much faster than the kinetic reaction rate and the homogeneous model may be applied. When $M^2>>1$, the kinetic reaction rate is much faster than the diffusion rate and the reaction rate is therefore limited by diffusion. When the diffusion and kinetic reaction rates are of the same order of magnitude ($M^2\sim1$), then Eqs. (3.3) and (3.4) must be simultaneously solved in their full form.

Diffusion-Limited Reaction Model

From calorimetric measurements on "starved-electrolyte" nickel electrodes, M^2 appears to be much greater than one.[5] Thus, the psuedo steady-state approximation of the hydrogen mass balance leads to

$$\frac{\partial^2\phi_1}{\partial\xi^2} = \frac{\partial^2 C_1}{\partial x^2} \approx 0 \tag{3.5}$$

Integration of Eq. (3.5) results in the psuedo steady-state approximation of a constant flux with respect to the spatial x-coordinate.

$$N_1 = -D_e\frac{dC_1}{dx} = constant \tag{3.6}$$

The instantaneous consumption rate of hydrogen is then given by

$$-\frac{dn_1}{dt} = S\left(-D_e\frac{dC_1}{dx}\right) \tag{3.7}$$

Integration of Eq. (3.6) from x = 0 to x = x_f and noting that $C_1 = C_{1,s}$, and $C_1 = 0$, respectively, yields the following equation for the hydrogen concentration distribution.

$$C_1 = C_{1,s}\left(1 - \frac{x}{x_f}\right) \tag{3.8}$$

Equation (3.7) reduces to

$$\frac{dn_1}{dt} = -\frac{SD_eC_{1,s}}{x_f} \tag{3.9}$$

A mass balance on the nickel oxyhydroxide yields

$$-\frac{dn_2}{dt} = S\rho_2\frac{dx_f}{dt} = -2\frac{dn_1}{dt} \tag{3.10}$$

Substituting Eq. (3.9) into Eq. (3.10) yields

$$\frac{dx_f}{dt} = 2\frac{D_eC_{1,s}}{\rho_2 x_f} \tag{3.11}$$

The concentration of hydrogen in the electrolyte at the interface (x=0) is given by Henry's Law as shown below.

$$P_1 = HC_{1,s} \tag{3.12}$$

From geometrical considerations

$$X_2 = \frac{x_f}{L_a} \tag{3.13}$$

Substituting Eqs. (3.12) and (3.13) into Eq. (3.11) yields

$$\frac{dX_2}{dt} = \frac{2D_e P_1}{H\rho_2 X_2 L_a^2} \tag{3.14}$$

For constant hydrogen pressure systems, integration of Eq. (3.14) yields the fraction unconverted of nickel oxyhydroxide as shown below.

$$1 - X_2 = 1 - \sqrt{\frac{4D_e P_1 t}{H\rho_2 L_a^2}} \tag{3.15}$$

For a constant hydrogen pressure battery of an initial fully-charged capacity of A_o, the capacity with time, A, is then given by

$$A = A_o(1 - X_2) = A_o\left(1 - \sqrt{\frac{4D_e P_1 t}{H\rho_2 L_a^2}}\right) \tag{3.16}$$

Thus, a plot of remaining capacity versus the square-root of open-circuit self-discharge time should yield a straight line.

For constant volume batteries, the fractional conversion of hydrogen and the nickel oxyhydroxide may be defined as

$$X_1 = X_2 = \frac{P_{1,o} - P_1}{P_{1,o} - P_{1,p}} \tag{3.17}$$

Thus,

$$\frac{dX_2}{dt} = \left(\frac{-1}{P_{1,o} - P_{1,p}}\right)\left(\frac{dP_1}{dt}\right) \tag{3.18}$$

Substituting Eq. (3.17) into Eq. (3.13) yields

$$\left(\frac{P_{1,o} - P_1}{P_1}\right)\frac{dP_1}{dt} = \frac{-2D_e(P_{1,o} - P_{1,p})^2}{H\rho_2 L_a^2} \tag{3.19}$$

Integration of Eq. (3.18) from t=0 to t and noting that P_1=$P_{1,o}$ to P_1, respectively, yields the following equation.

$$\ln\left(\frac{P_1}{P_{1,o}}\right) - \left(\frac{P_1 - P_{1,o}}{P_{1,o}}\right) = -\left(\frac{2D_e(P_{1,o} - P_{1,p})^2}{H\rho_2 L_a^2 P_{1,o}}\right)t \tag{3.20}$$

Thus, a plot of the left-hand-side of Eq. (3.19) versus time would yield a straight line.

NUMERICAL MODEL

Analytical solutions to Eqs. (3.1) and (3.2) are only possible for first order reactions under limiting conditions in which the pseudo steady-state approximation is valid or for entirely diffusion-limited or kinetically-limited reactions.[17,18] However, second order reactions require a numerical solution. Assuming constant diffusivity and porosity, Eqs. (3.1) and (3.2) were solved using the Crank-Nicolson implicit finite difference method with second order reaction kinetics. The program listing is given in the Appendix.

Numerical Model Finite Difference Equations

To put Eq. (3.3) into the Crank-Nicolson implicit finite difference form, the equation was algebraically manipulated to the equation shown below.

$$\frac{\partial \phi_1}{\partial t} = \left(\frac{D_e}{\varepsilon L_a^2}\right)\frac{\partial^2 \phi_1}{\partial \xi^2} - \frac{k_2}{\varepsilon}\phi_1 C_2 \tag{3.21}$$

Now, the Thiele modulus for a second order reaction becomes

$$M^2 = \frac{k_2 C_{2,o} L_a^2}{D_e} \tag{3.22}$$

Equation (3.21) can be simplified by defining two new variables alp and rate as shown below.

$$alp = \frac{D_e}{\varepsilon L_a^2} \tag{3.23}$$

$$rate = \frac{k_2}{\varepsilon} \tag{3.24}$$

Equation (3.21) in terms of Eqs. (3.23) and (3.24) then becomes

$$\frac{\partial \phi_1}{\partial t} = alp\frac{\partial^2 \phi_1}{\partial \xi^2} - rate\phi_1 C_2 \tag{3.25}$$

Now, by using Eqs. (3.22), (3.23), and (3.24), the variable rate can be determined as shown below.

$$rate = \frac{M^2 alp}{C_{2,o}} = \frac{M^2 D_e}{\varepsilon L_a^2 C_{2,o}} \tag{3.26}$$

Thus, for given values of diffusivity, porosity, active material length and concentration and an assumed value for the Thiele Modulus, a value for the variable rate is determined.

Now, the concentration of β-NiOOH in Eq. (3.25) is determined by Eq. (3.2). Equation (3.2) can be written as

$$\frac{\partial C_2}{\partial t} = -2k_2 C_1 C_2 = -2k_2 C_{1,s} \phi_1 C_2 \tag{3.27}$$

Thus, Eqs. (3.25) and (3.27) are coupled together by the reactant concentrations.

Equation (3.25) in the Crank-Nicolson implicit finite-difference form is shown below.

$$\frac{\phi_1^{i,n+1} - \phi_1^{i,n}}{\Delta t} = \frac{1}{2} alp \left(\frac{\phi_1^{i-1,n+1} - 2\phi_1^{i,n+1} + \phi_1^{i+1,n+1}}{\Delta x^2} \right) + \frac{1}{2} alp \left(\frac{\phi_1^{i-1,n} - 2\phi_1^{i,n} + \phi_1^{i+1,n}}{\Delta x^2} \right) - rate \phi_1^{i,n} C_2^{i,n} \tag{3.28}$$

Equation (3.27) in finite difference form is shown below.

$$\frac{C_2^{i,n+1} - C_2^{i,n}}{\Delta t} = -2k_2 C_{1,s} \phi_1^{i,n} C_2^{i,n} \tag{3.29}$$

Now, defining the variable λ

$$\lambda = \frac{\Delta t}{\Delta x^2} \tag{3.30}$$

and substituting λ into Eq. (3.28) and rearranging yields

$$-\frac{1}{2}(alp)(\lambda)\phi_1^{i-1,n+1} + (1 + (alp)(\lambda))\phi_1^{i,n+1} - \frac{1}{2}(alp)(\lambda)\phi_1^{i+1,n+1} = \phi_1^{i,n} - (\Delta t)(rate) C_2^{i,n} \phi_1^{i,n} + \frac{1}{2}(alp)(\lambda)(\phi_1^{i-1,n} - 2\phi_1^{i,n} + \phi_1^{i+1,n}) \tag{3.31}$$

At the interface between the hydrogen gas and the electrolyte/active material mixture, Eq. (3.31) becomes

$$(1 + (alp)(\lambda))\phi_1^{2,n+1} - \frac{1}{2}(alp)(\lambda)\phi_1^{3,n+1} =$$
$$\phi_1^{2,n} - (\Delta t)(rate)\phi_1^{2,n}C_2^{2,n} + \frac{1}{2}(alp)(rate)(2\phi_1^{1,n} - 2\phi_1^{2,n} + \phi_1^{3,n}) \quad (3.32)$$

And at the interface between the current collector and the electrolyte/active material Eq. (3.31) becomes

$$-\frac{1}{2}(alp)(\lambda)\phi_1^{k-2,n+1} + \left(1 + \frac{(alp)(\lambda)}{2}\right)\phi_1^{k-1,n+1} =$$
$$\phi_1^{k-1,n} - (\Delta t)(rate)\phi_1^{k-1,n}C_2^{k-1,n} + \frac{1}{2}(alp)(\lambda)(\phi_1^{k-2,n} - \phi_1^{k-1,n}) \quad (3.33)$$

Equations (3.31)-(3.33) are then solved by the use of the Thomas Algorithm and Eq (3.29) is used to explicitly update the concentration of the β-NiOOH.

Numerical Model Solution Scheme

The input values needed for the numerical model given in the Appendix and the input values used to generate Fig. 32 are

i) value of the number of dimensionless distance points; variable K=51

ii) value of the number of time points; variable ZZ=30001

iii) value of the effective diffusion coefficient divided by the porosity; variable DE=1E-11 cm^2/sec

iv) value of the active material length; variable LE=2E-4 cm

v) value of the Thiele Modulus; variable TM=50

vi) value of the Battery Temperature in Kelvin; variable T=283.15K

vii) value of the initial battery pressure; variable BP=257.5 PSIA

viii) value of the precharge battery pressure; variable BPP=104 PSIA

ix) value of the battery gas volume; variable BVOL=2.342 liters

From these input values, the following calculations are performed.

i) determination of dimensionless distance stepsize; variable DELTAX

ii) determination of time stepsize; variable DELTAZ

iii) determination of variable λ; variable LAMDA

iv) determination of variable alp; variable ALP

v) determination of variable rate; variable RATE

vi) determination of hydrogen gas compressibility factor by the use of the virial equation of state for hydrogen; variable ZZ

vii) determination of dissolved hydrogen concentration at x=0 and t=0 by the use of Henry's Law; variable CDISO

viii) determination of amount of hydrogen in battery at t=0; variable NHO

ix) determination of amount of hydrogen precharge; variable NHP

After these initial calculations are performed, the initial condition for hydrogen and β-NiOOH concentrations within the active material/electrolyte mixture are set. For the full charge condition, the hydrogen concentration within the mixture will be zero except at the x=0 where the dimensionless hydrogen concentration is set to 1. The β-NiOOH concentration at full-charge is set to the molar density measured for this battery active material.

After the initial conditions are set, a file named 'OUT' is opened for sequential storage.

The first step in the body of the program is to determine, by the use of the counter variables M and Z, if the values calculated in the body of the program, such as the concentrations of hydrogen and β-NiOOH and the fractional conversion of β-NiOOH, should be printed or if the program execution should stop. The next step, by the use of the Thomas Algorithm, is to calculate the hydrogen concentrations. By use of Eq. (3.29), the β-NiOOH concentrations are then calculated explicitly.

After the concentrations are determined, the fractional conversion of β-NiOOH is calculated by numerically integrating the β-NiOOH concentration by the Simpson Method.

Based on the fractional conversion, the battery pressure is then updated and a new interfacial dissolved hydrogen concentration is then determined by the use of Henry's Law.

The program is then terminated after one day of simulation. By modifying the definition of DELTAZ, fraction of a day or multiple days may be simulated.

CHAPTER IV

EXPERIMENTAL DESCRIPTION AND METHODS

Figure 2 shows the overall arrangement of the experimental apparatus used in this investigation. The pressure vessel houses the nickel hydrogen battery. Copper coils from the constant temperature water circulating bath encapsulate the pressure vessel. A blanket of insulation was used to insulate the pressure vessel. Thermocouple, electrical, and pressure transducer leads are shown extending from the pressure vessel. The constant temperature water bath is seen below the pressure vessel.

Electrical cycling of the cell and data acquisition were accomplished using the Hewlett-Packard HP 1000E series mainframe computer and the HP 3497A data acquisition/control unit shown in Figs. 3 and 4, respectively. The raw data consisted of time of reading, cell temperature, cell pressure and cell voltage. This raw data was then utilized in a Lotus 1-2-3 spreadsheet program on a Zenith Z-386 personal computer, shown in Fig. 5, for further processing.

Constant current charge periods were manually determined by cell voltage roll-over, a given cell voltage, or a given charge time. After a given period of open-circuit time, the cell was discharged at a constant current to a cell voltage of 1.0 volts.

The current through the cell was measured with a 100 mV, 0.1 amperes shunt and voltage was measured directly on the terminals of the cell. Pressure was sensed with a Data Instruments Model AB500 pressure transducer.

Figure 2. Cell, Cell Insulation, and Circulator Bath.

Figure 3. Hewlett-Packard HP 1000E Mainframe Computer.

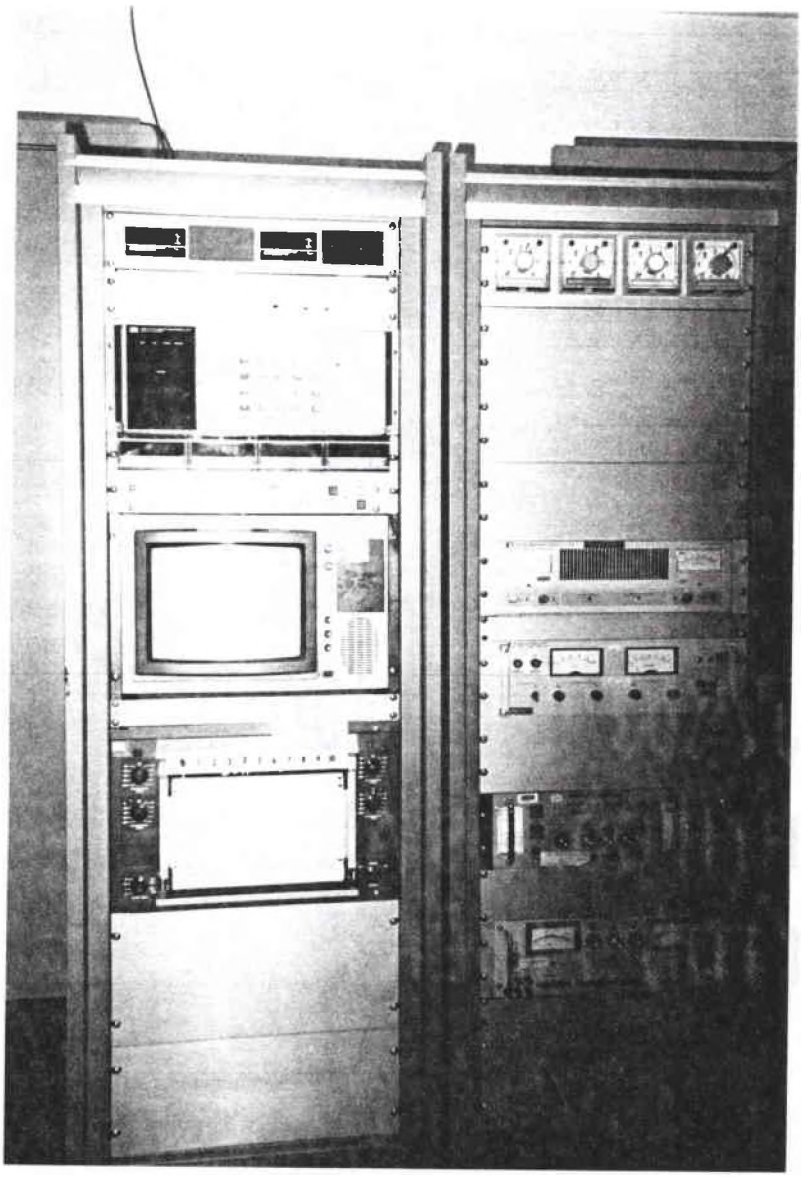

Figure 4. Hewlett-Packard HP 3497A Data Acquisition/Control Unit.

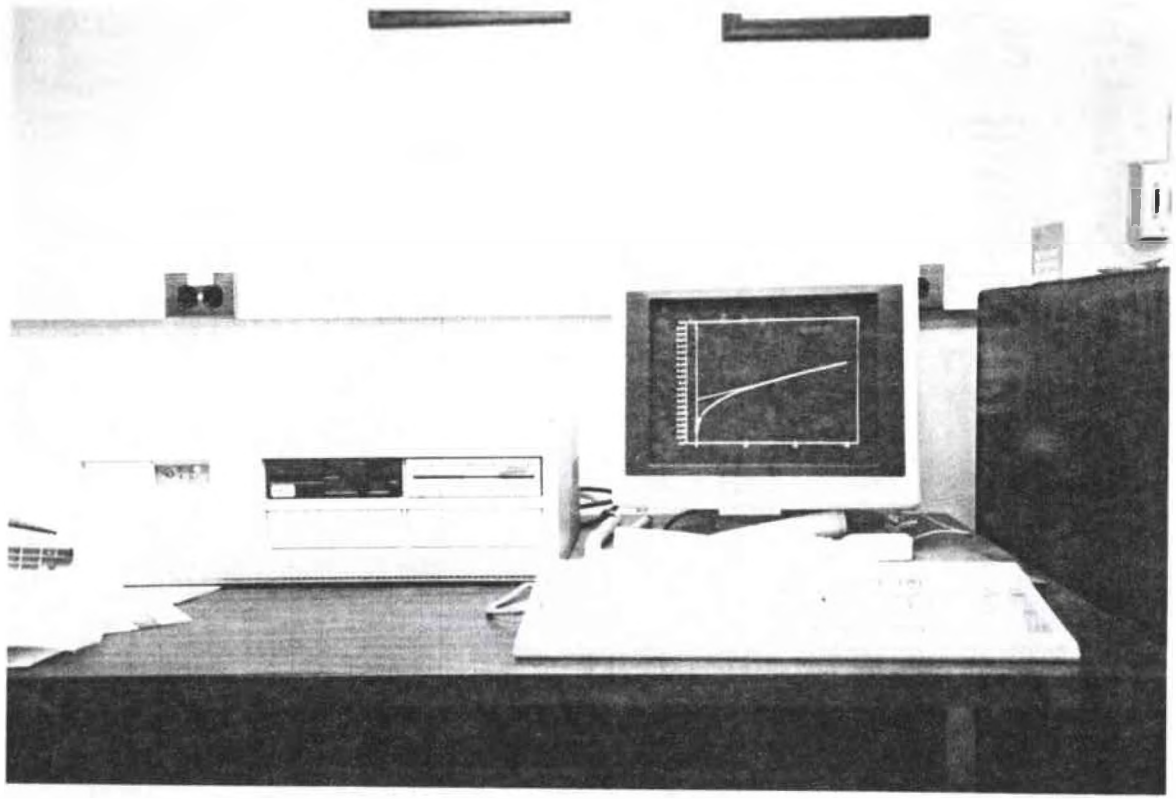

Figure 5. Zenith Z-386 Personal Computer with 80387 Co-processor.

The temperature of the cell was regulated by the use of a Polyscience Model 9500 constant temperature circulator bath. The temperature of the cell was sensed by a copper-constantan Type T thermocouple which was housed inside the pressure vessel.

CHAPTER V

EXPERIMENTAL RESULTS

To verify the proposed mathematical model, experimental measurements on the open-circuit self-discharge behavior of a 54.7 amp-hour nickel hydrogen cell were performed. Absolute cell pressure, corrected for gas compressibility and temperature (corrected pressure) determines the amount of hydrogen present in the cell and thus the extent of the self-discharge reaction. Thus, the cell pressure and temperature were monitored on open-circuit.

To "fully" charge the cell, a constant current charge was applied until the cell voltage stopped increasing and started to decrease. This is defined as "voltage-rollover" in the battery industry and is a good indicator for termination of charging for nickel-hydrogen batteries. Corrected pressure versus open-circuit time for the cell fully charged at 11.52 amps (C/4.75 rate) at 11°C is presented in Fig. 6. Data for the cell fully charged at 44 amps (C/1.24 rate) at 21°C is presented in Fig. 7. Data for the cell partially charged (~3/4 full charge) at the C/4.75 charge rate at 11°C, 21°C, and 30°C is presented in Figs. 8, 9, and 10, respectively. Fraction of full charge is defined as time of charge at C/4.75 rate divided by 4.75 hours. And data for the cell roughly half-charged (C/4.75 rate for 2.5 hours) at 13°C is presented in Fig. 11.

A typical C/4.75 charge curve at 11°C is presented in Fig. 12. A typical C/2 discharge rate curve following an open-circuit period is shown in Fig. 13.

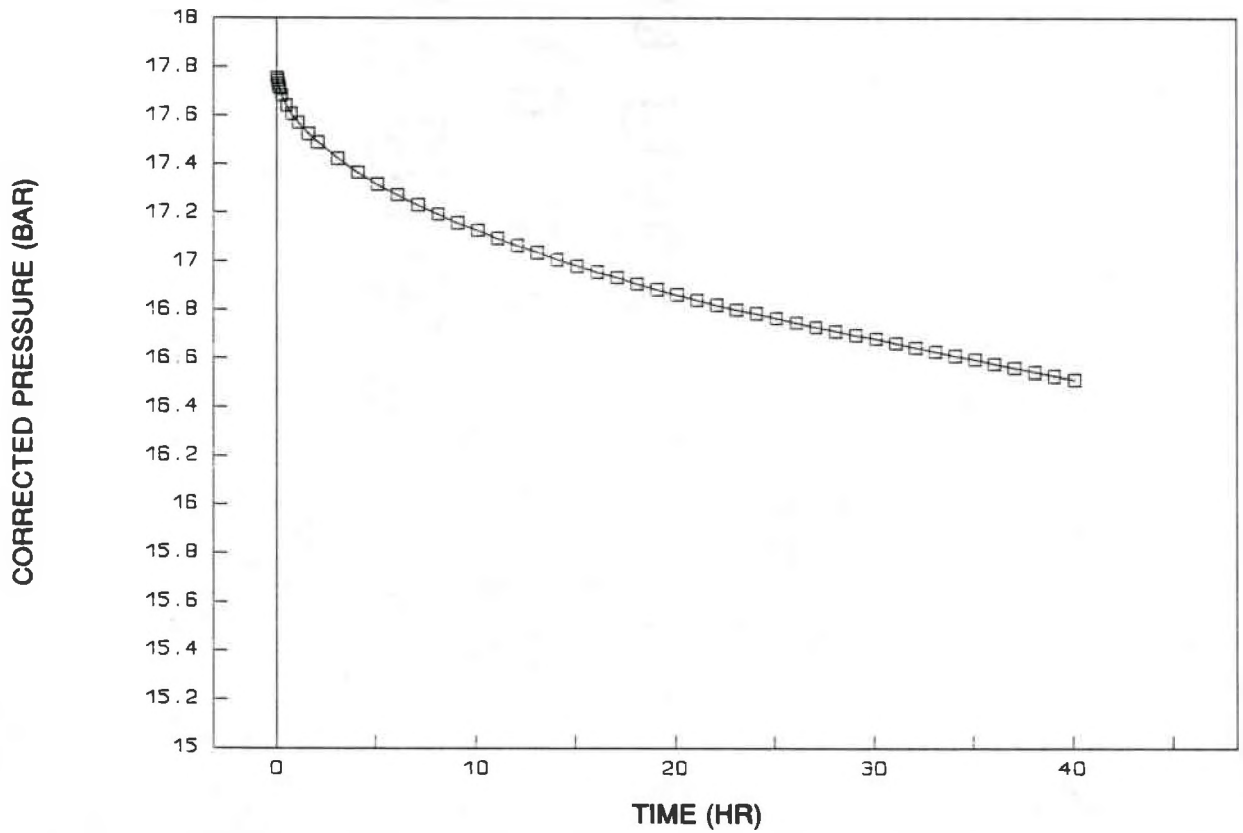

Figure 6. Corrected Pressure versus Time at 11°C for Initial Full Charge.

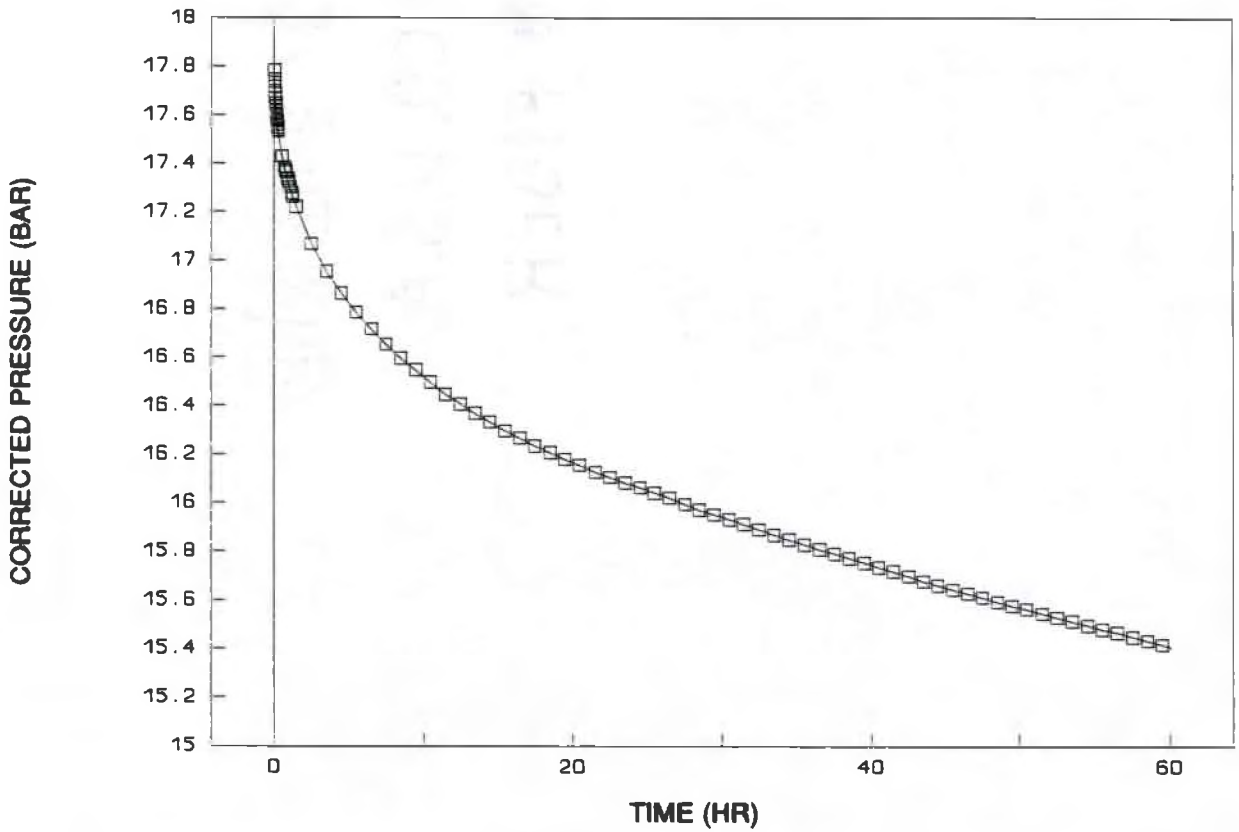

Figure 7. Corrected Pressure versus Time at 21°C for Initial Full Charge.

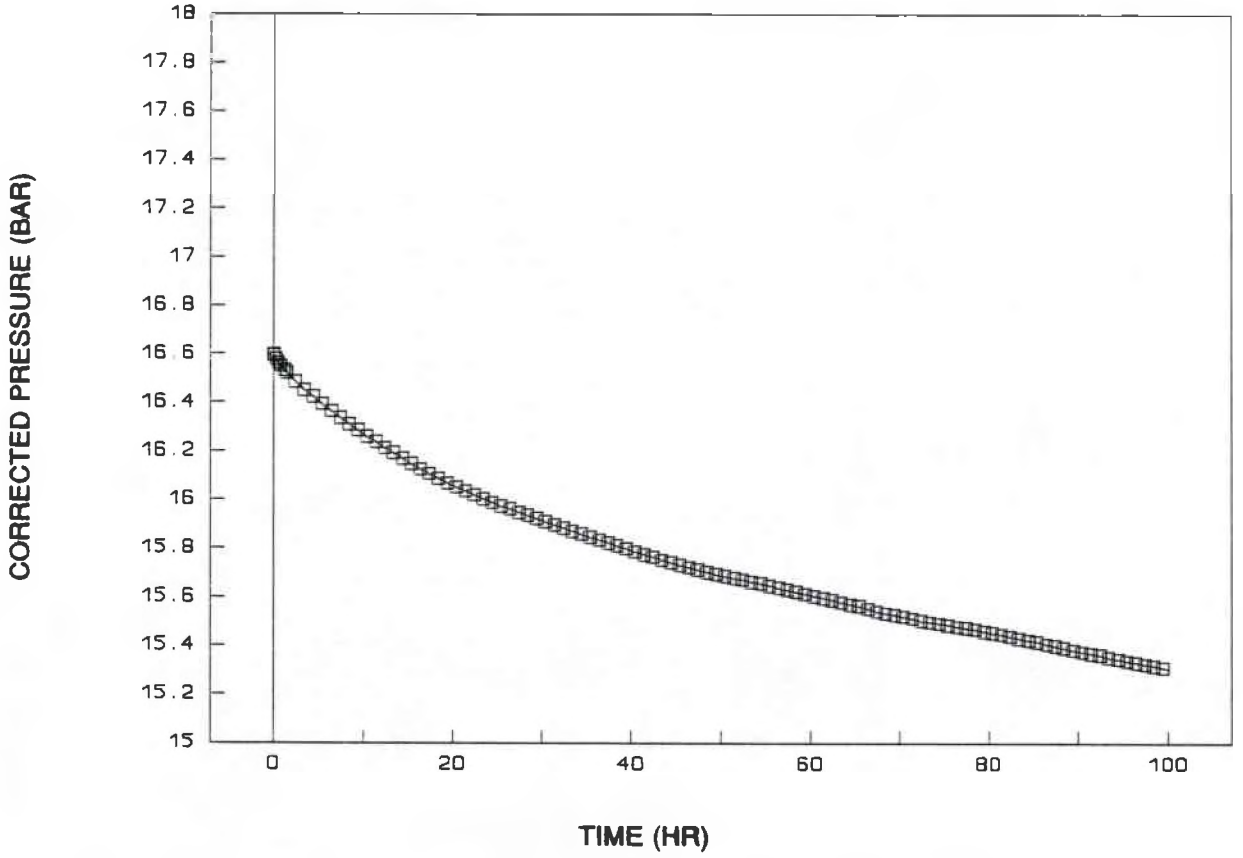

Figure 8. Corrected Pressure versus Time at 11°C for Initial 81% Full Charge.

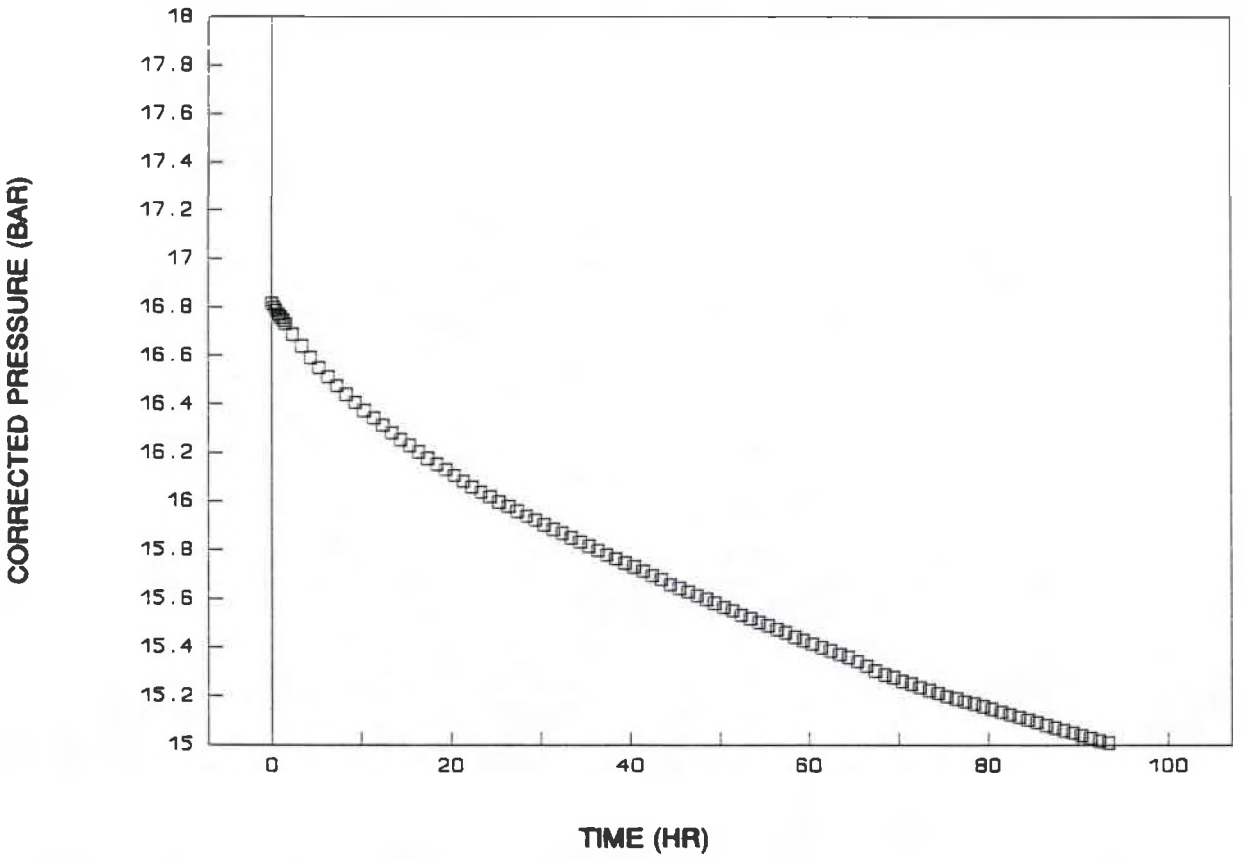

Figure 9. Corrected Pressure versus Time at 21°C for Initial 78% Full Charge.

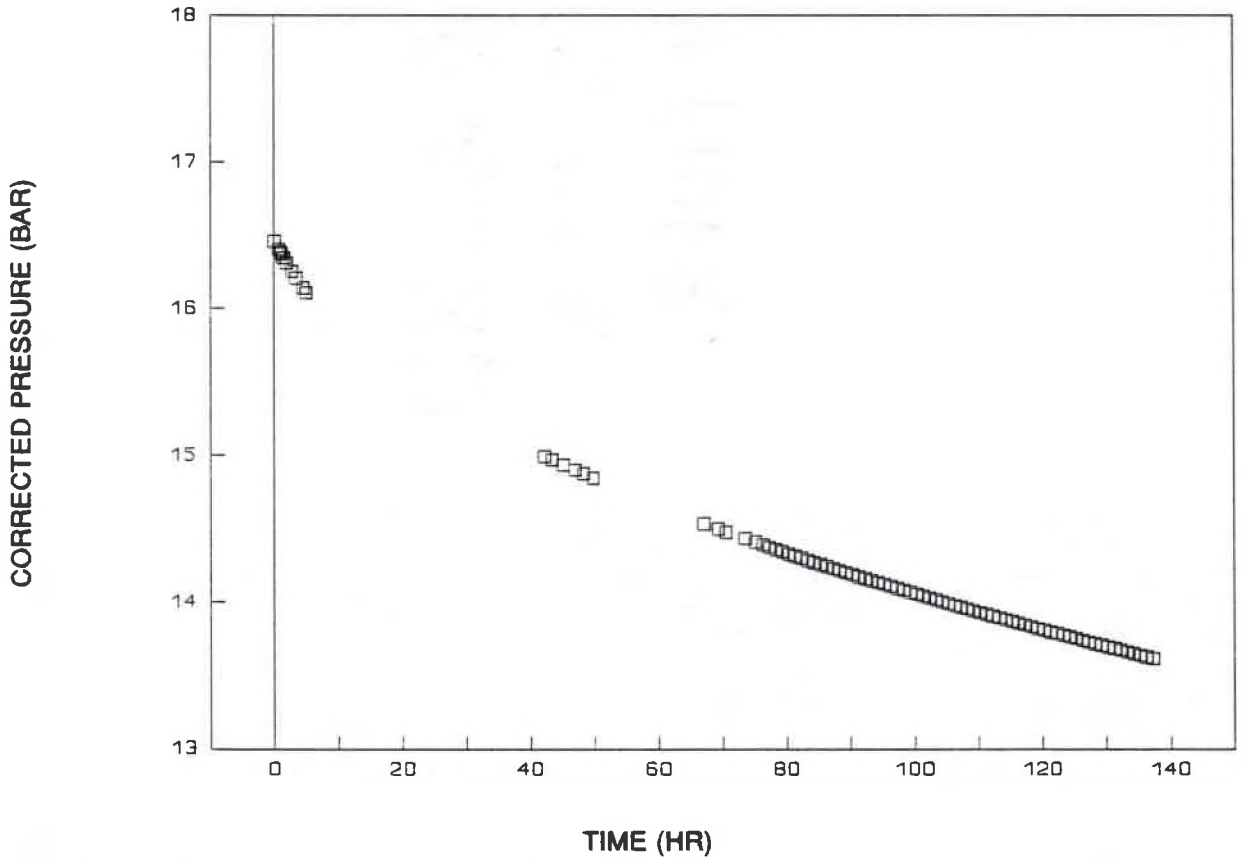

Figure 10. Corrected Pressure versus Time at 30°C for Initial 76% Full Charge.

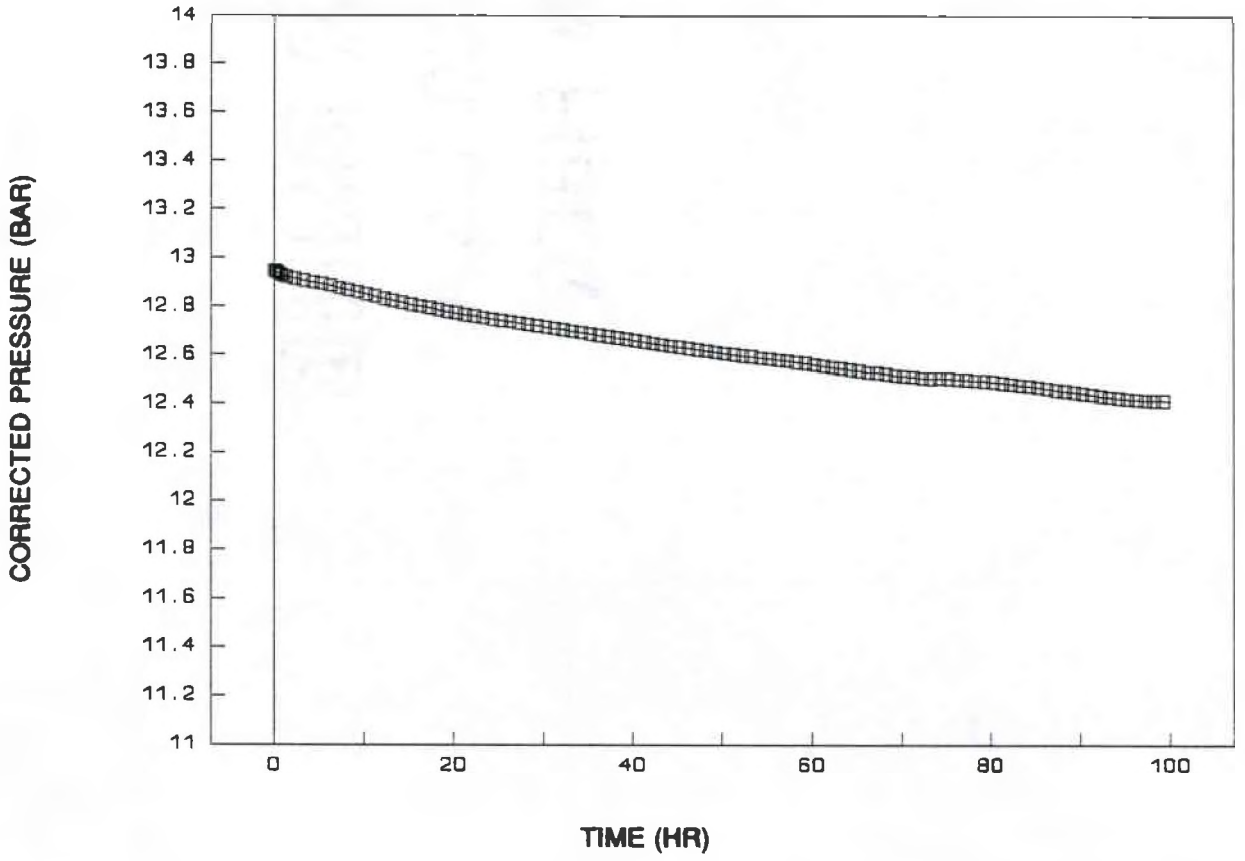

Figure 11. Corrected Pressure versus Time at 13°C for Initial 53% Full Charge.

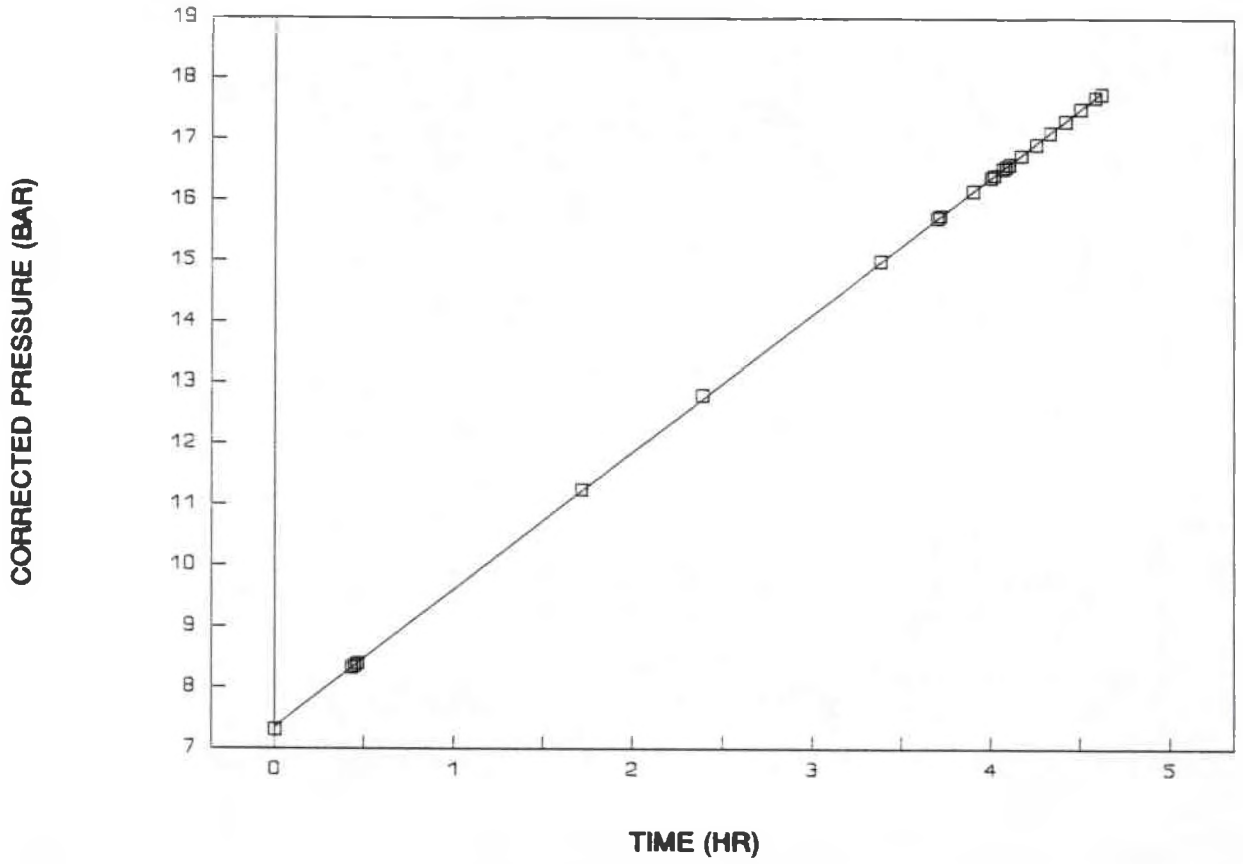

Figure 12. C/4.75 Charge Rate (11.52 amps) at 11°C.

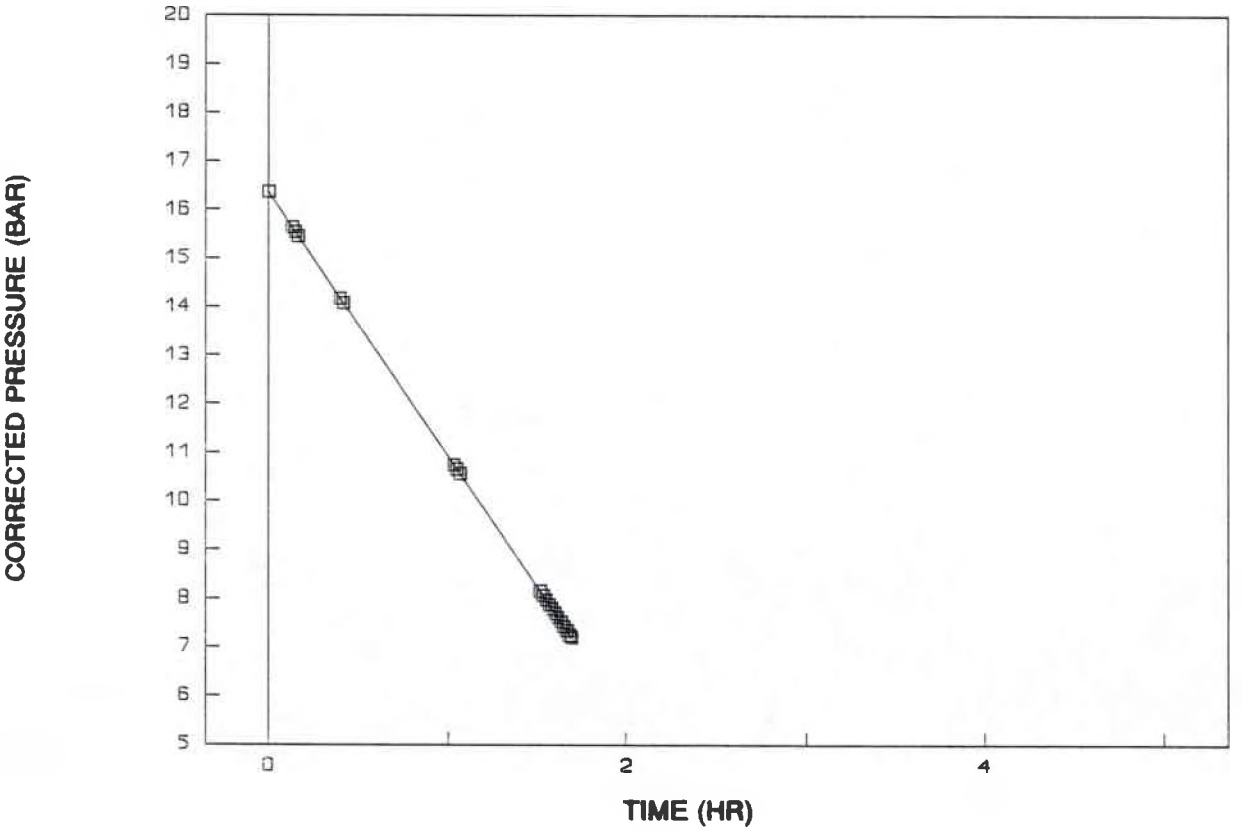

Figure 13. C/2 Discharge Rate at 13°C.

CHAPTER VI

COMPARISON OF EXPERIMENTAL RESULTS WITH MODEL PREDICTIONS

To verify the assumption that diffusion limits the self-discharge reaction ($M^2>>1$) for nickel hydrogen, Eq. (3.20) was applied to the experimental data presented in Figs. 6-11. To show that $M^2<<1$ is unlikely, Eqs. (2.6) and (2.10) are also applied to the experimental data. Finally, the numerical model is also used to verify the validity of the assumption that $M^2>>1$.

$M^2>>1$; Diffusion-Limited Reaction Model

Equation (3.20) was applied to the data of Figs. 6-11. The results are presented in Figs. 14-19, respectively. For the full charge case at 11°C shown in Fig. 14, a straight line relationship resulted as predicted.

Figure 15 shows a straight line relationship after a period of approximately 20 hours. This deviation at short times is, perhaps, the result of oxygen being produced at the end of charge. Oxygen production is more noticeable as the cell charge temperature increases.[3]

For the partially charged cases (~75%) shown in Figs. 16-18, a straight relationship results after a period of approximately 20 hours. This deviation at short times indicates a drop in M^2 due to the lower β-NiOOH concentration.

For the half-charged case at 13°C shown in Fig. 19, a straight line relationship results after a period of approximately 40 hours. This deviation is again due to a further reduction in M^2 as a result of a lower β-NiOOH concentration.

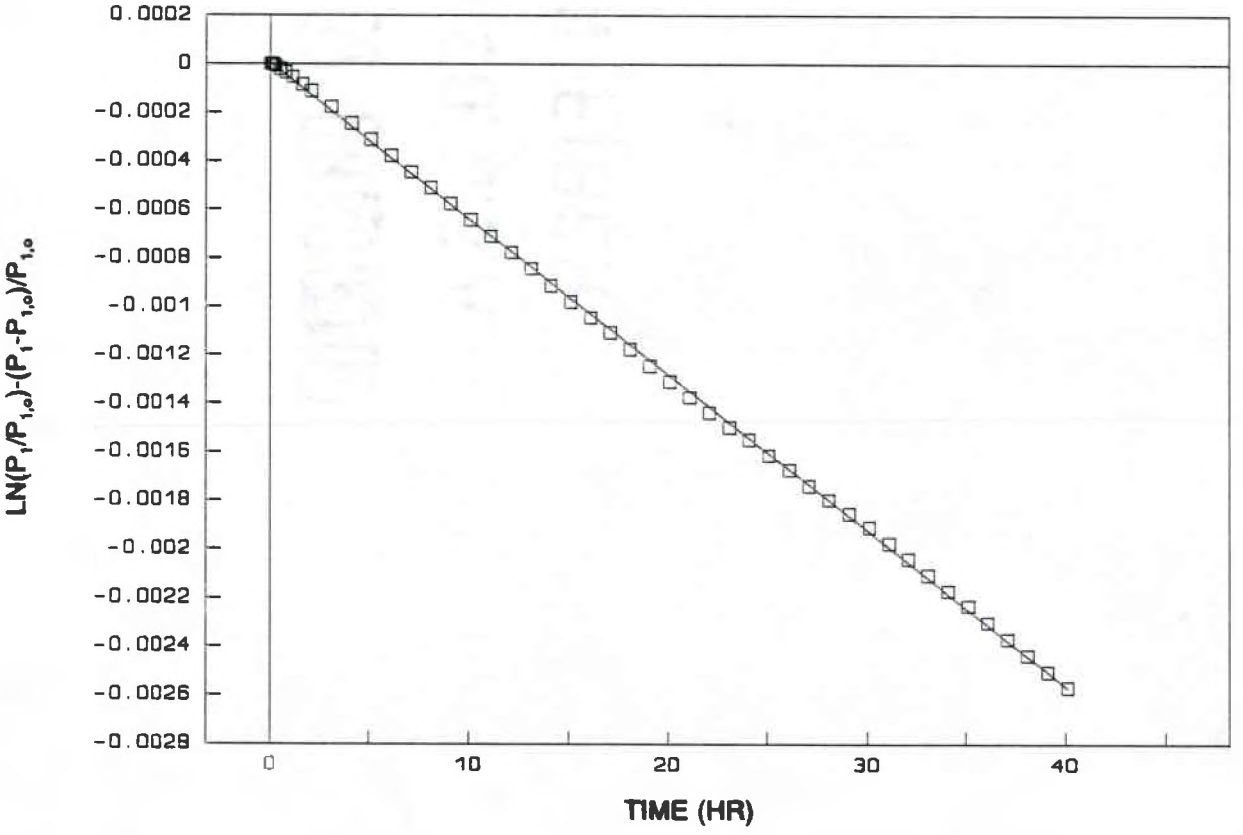

Figure 14. Correlation of M^2>>1 at 11°C

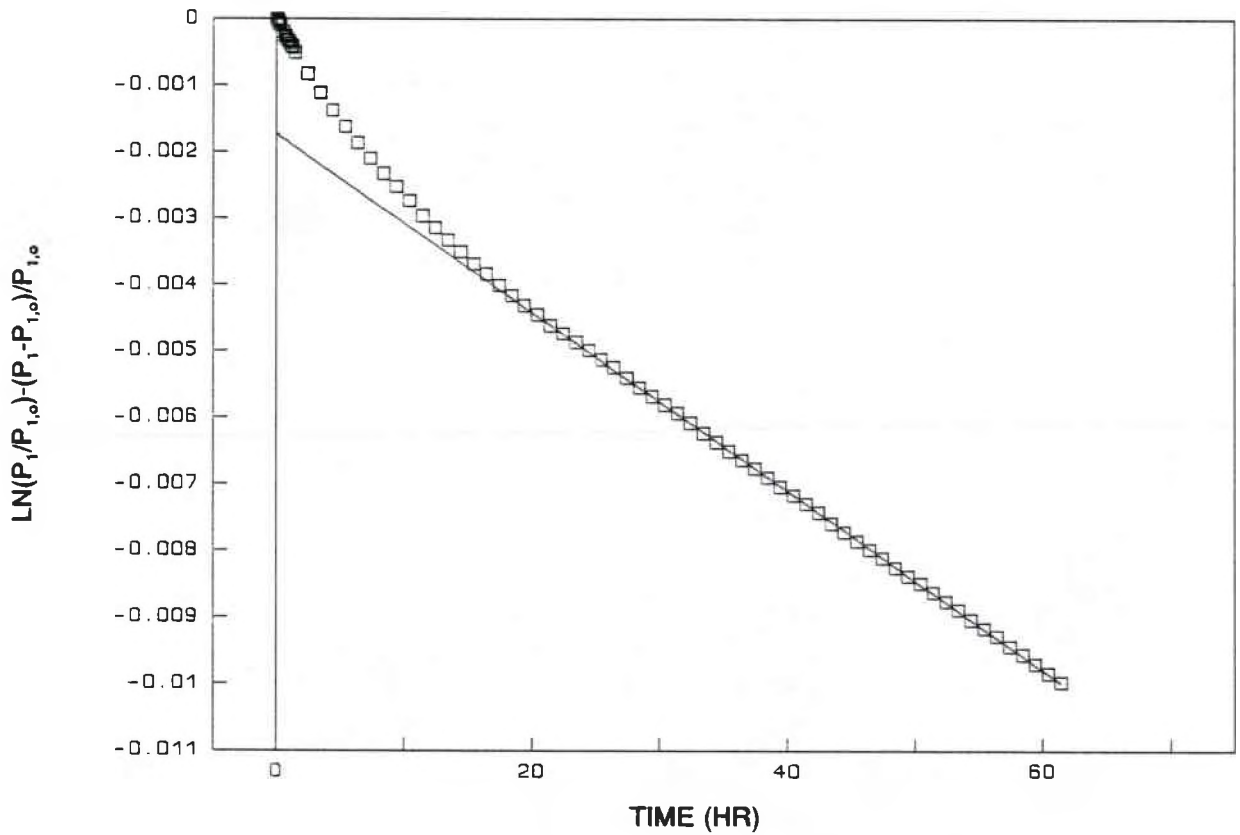

Figure 15. Correlation of $M^2>>1$ at 21°C

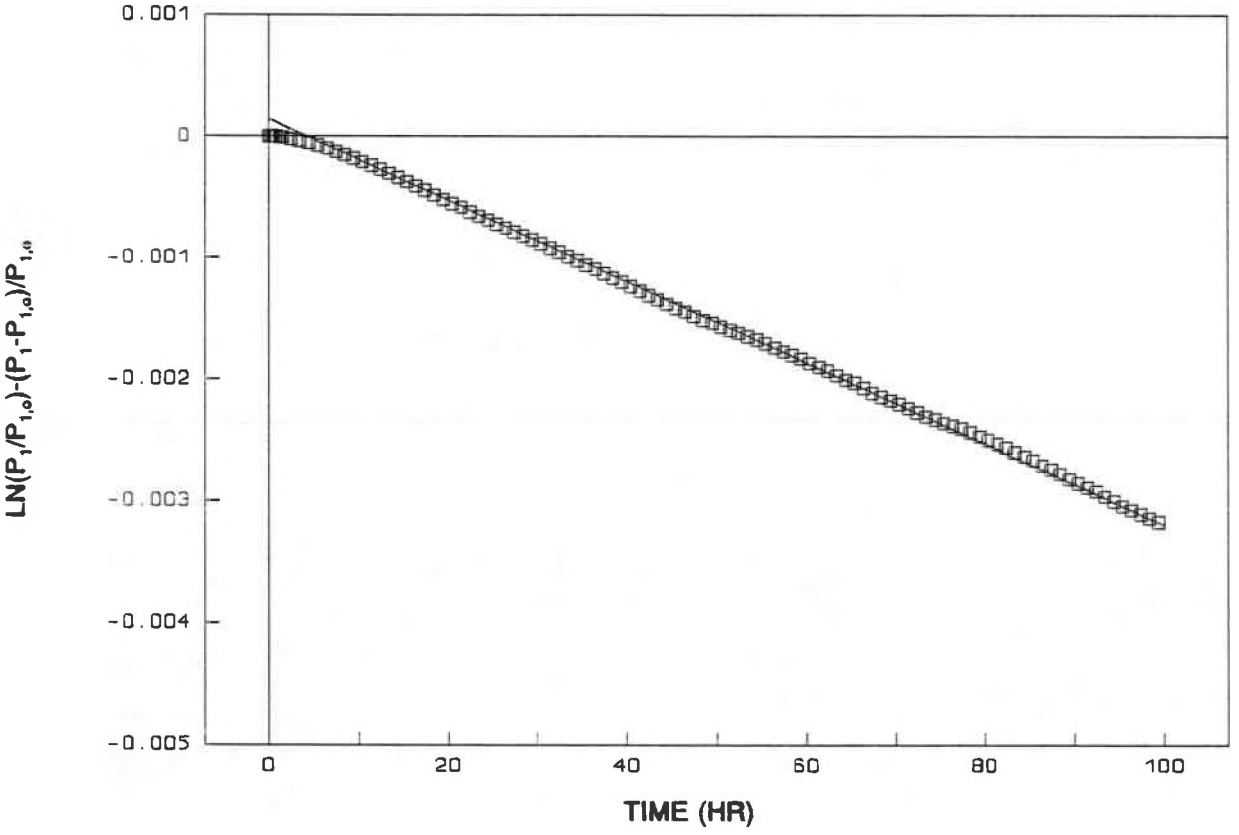

Figure 16. Correlation of $M^2>>1$ at 11°C for Initial 81% Full Charge.

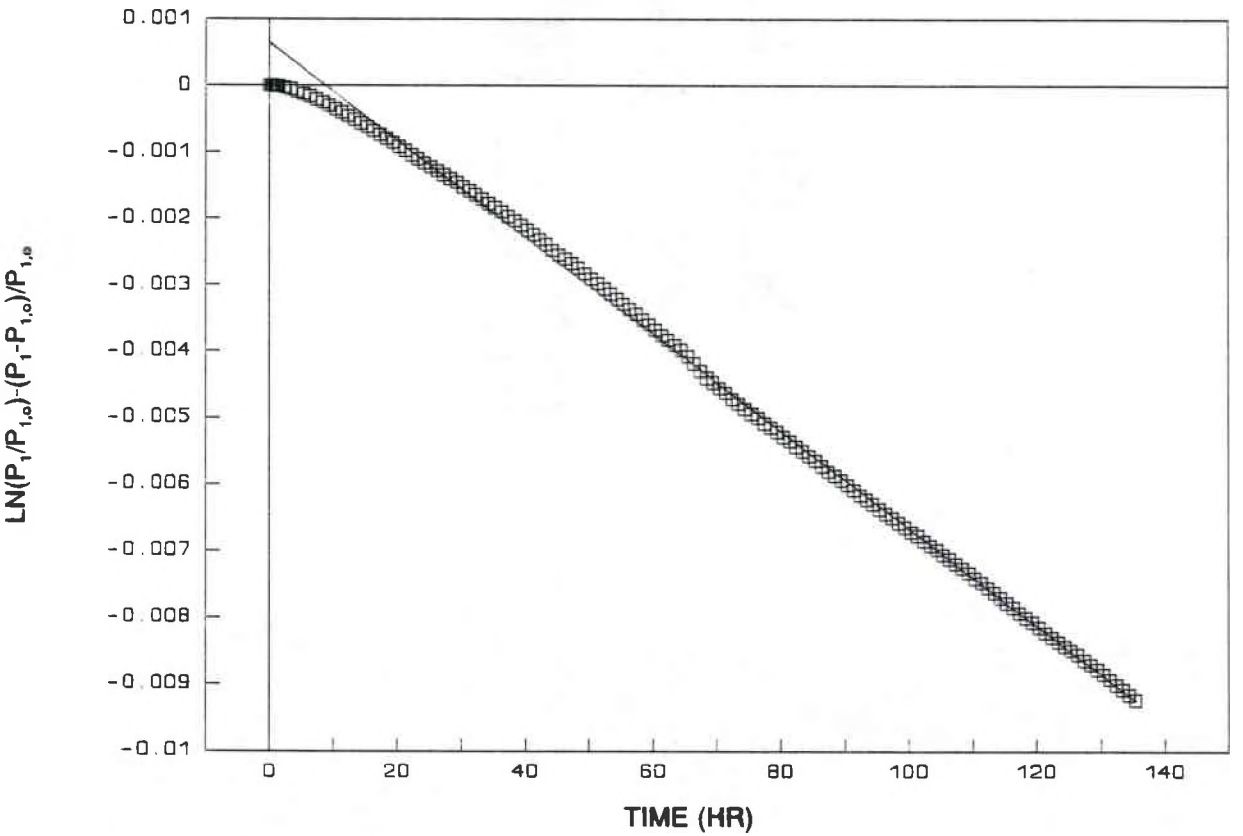

Figure 17. Correlation of $M^2>>1$ at 21°C for Initial 78% Full Charge.

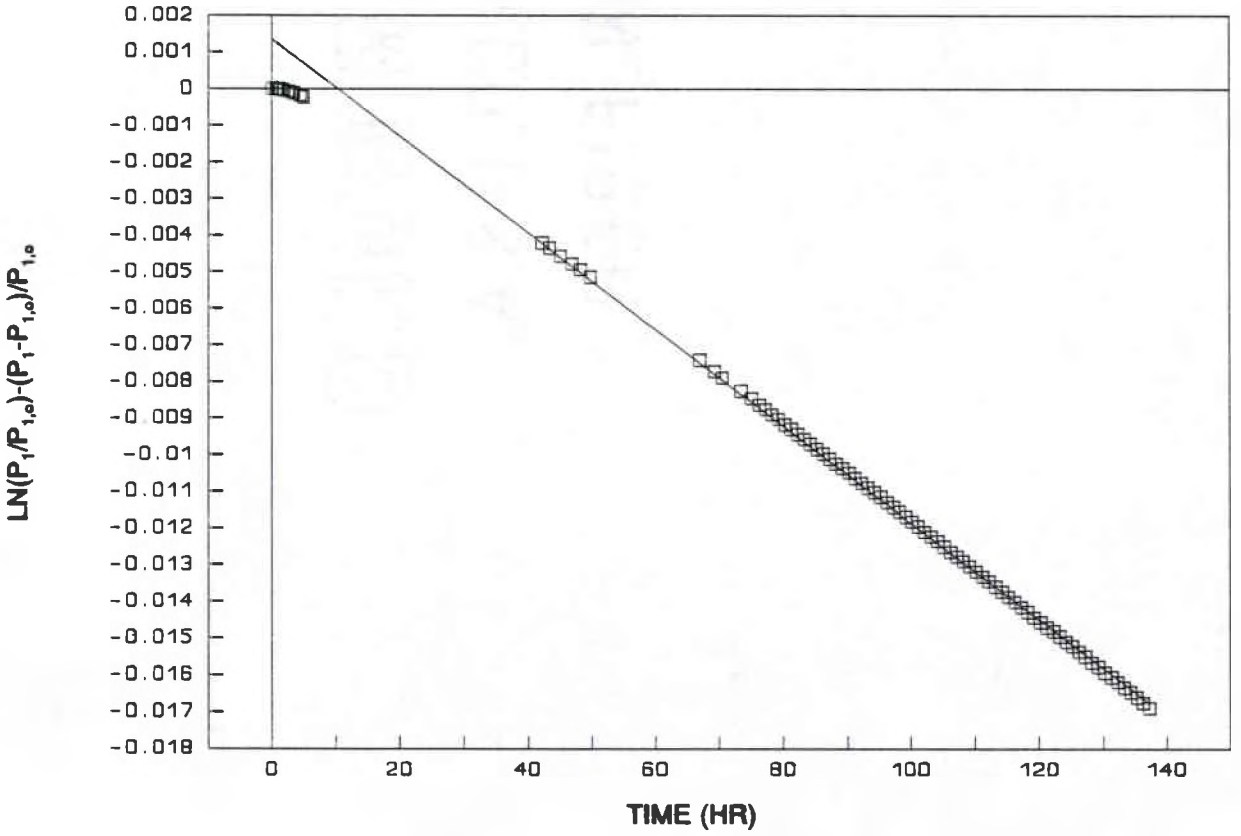

Figure 18. Correlation of $M^2>>1$ at 30°C for Initial 76% Full Charge.

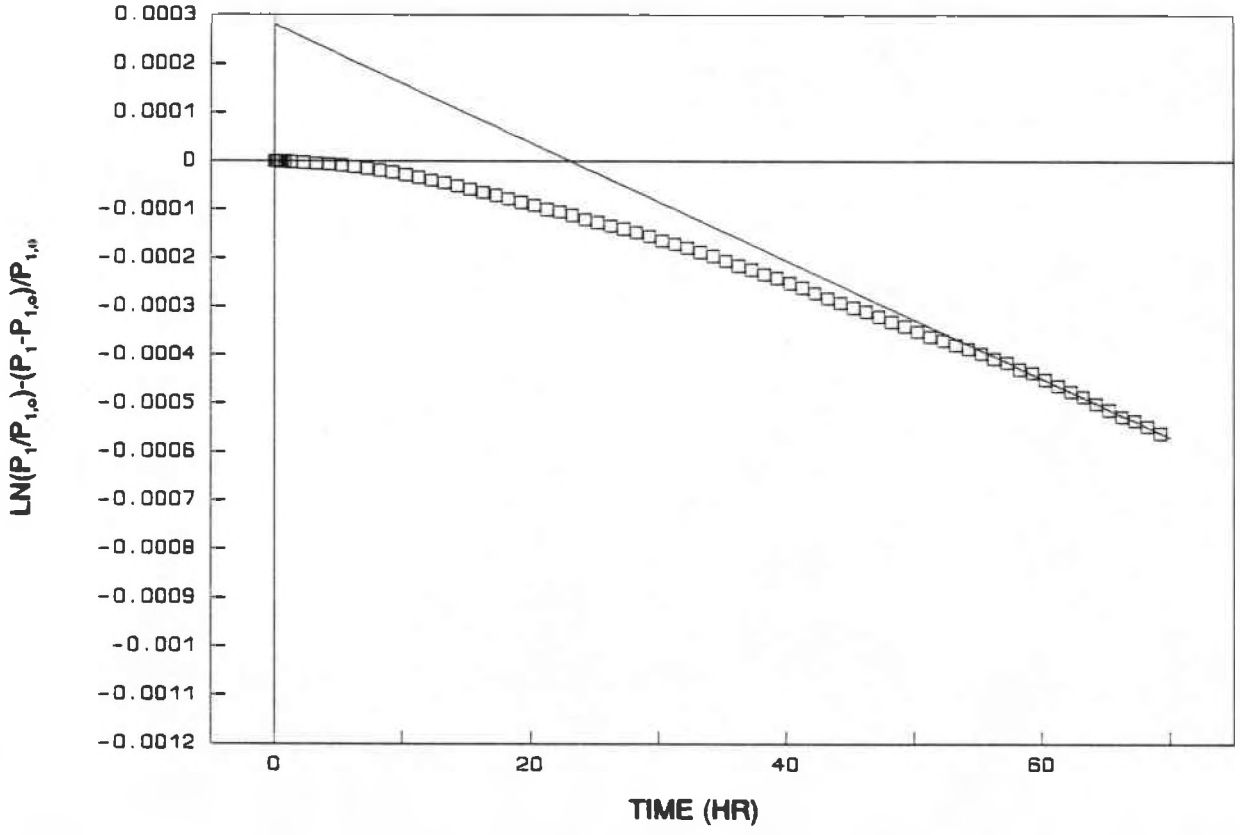

Figure 19. Correlation of $M^2>>1$ at 13°C for Initial 53% Full Charge.

$M^2 \ll 1$; HOMOGENEOUS REACTION MODEL

Assuming the kinetics are first order with respect to hydrogen, Eq. (2.6) was applied to the results presented in Figs. 6-11 and is shown in Figs. 20-25.

Figure 20 indicates a deviation at short times from the proposed first order kinetic model. However, a change in the charge slope did not occur prior to open-circuit. Therefore, it is not reasonable to conclude that the deviation observed at short times for this case is the result of excess oxygen.

Excess oxygen was produced, however, for the curve represented by Fig. 21. But, the charge slope did not change for the data represented by Figs. 22-25 and thus to conclude that oxygen is the culprit for the deviation for all of these cases is not reasonable.

Assuming second order kinetics, first order with respect to hydrogen and first order with respect to β-NiOOH, Eq. (2.10) was applied to the results presented in Figs. 6-11 and is shown in Figs. 26-31.

The same rationale used to explain first order kinetics may also be used for second order kinetics since oxygen is required to explain the higher rates observed at short times for both cases.

Figure 20. First Order Kinetics at 11°C.

Figure 21. First Order Kinetics at 21°C.

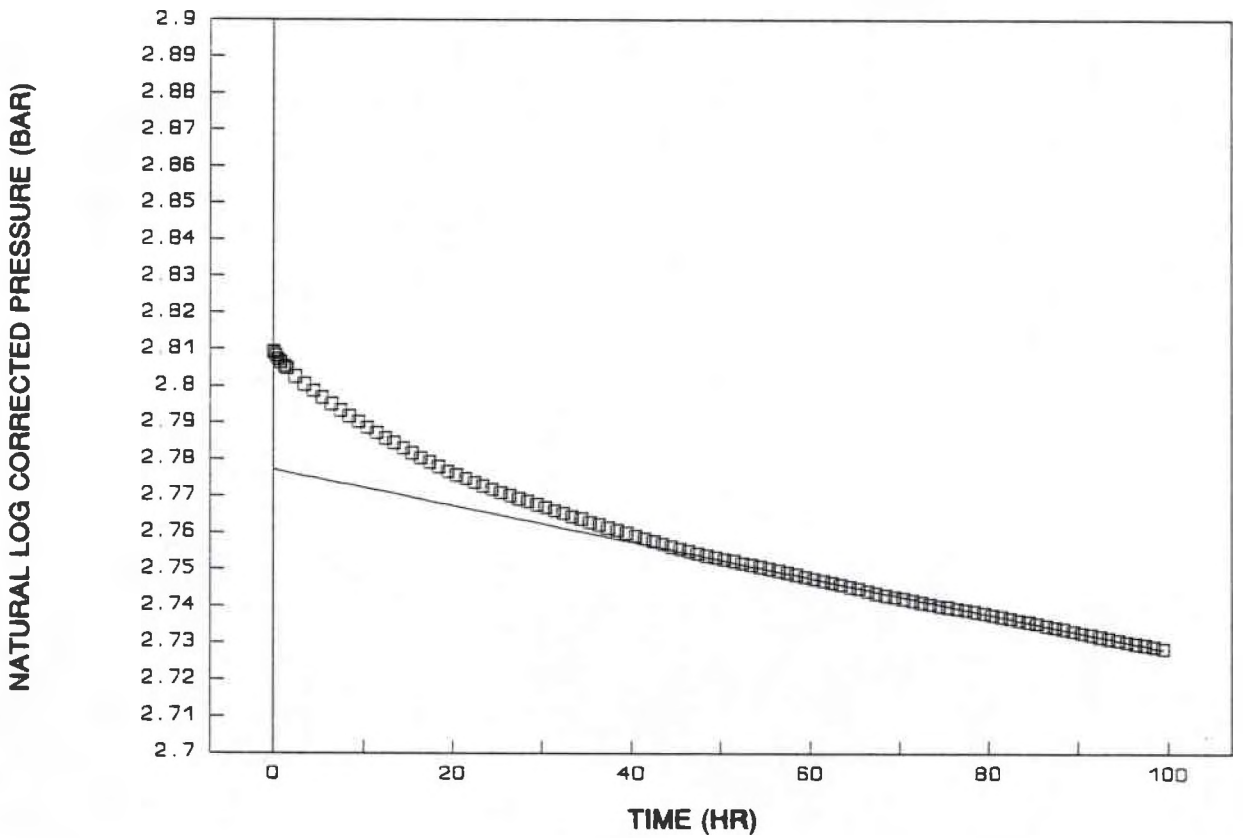

Figure 22. First Order Kinetics at 11°C for Initial 81% Full Charge.

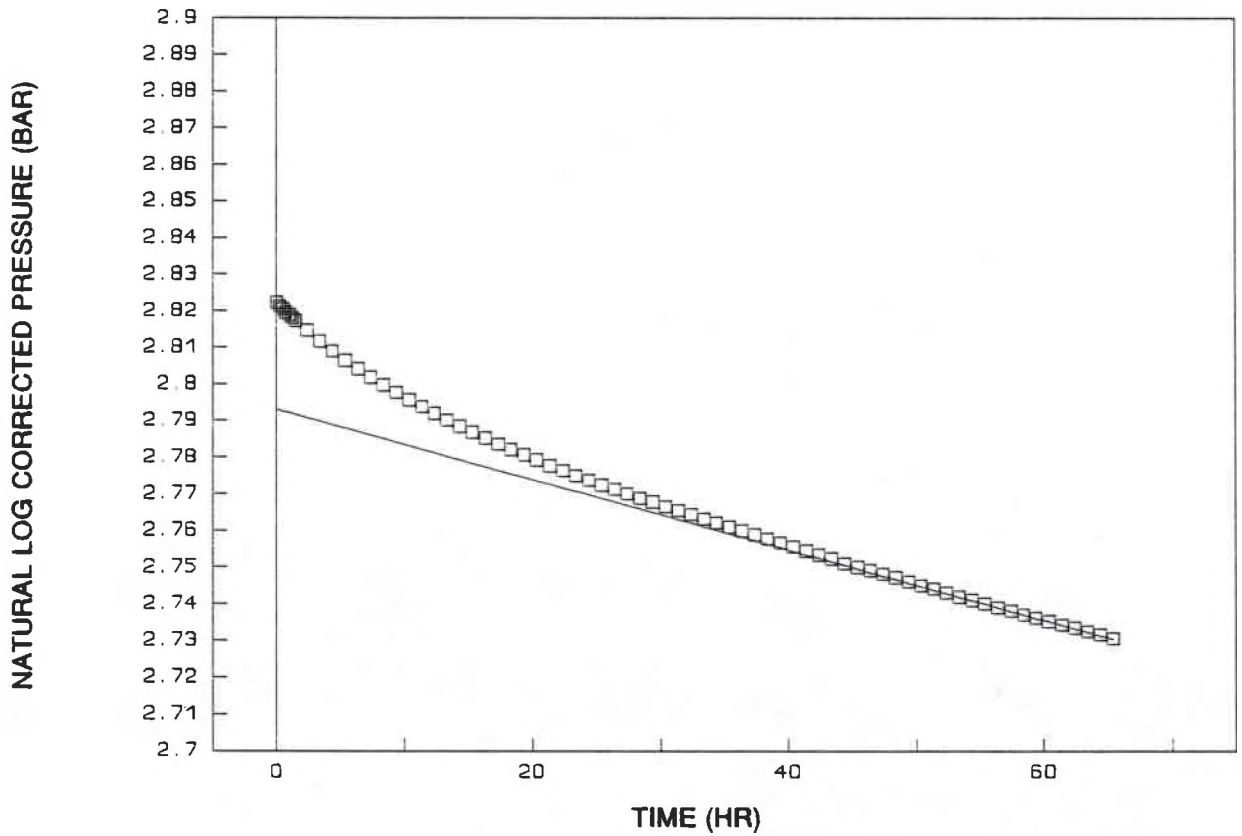

Figure 23. First Order Kinetics at 21°C for Initial 78% Full Charge.

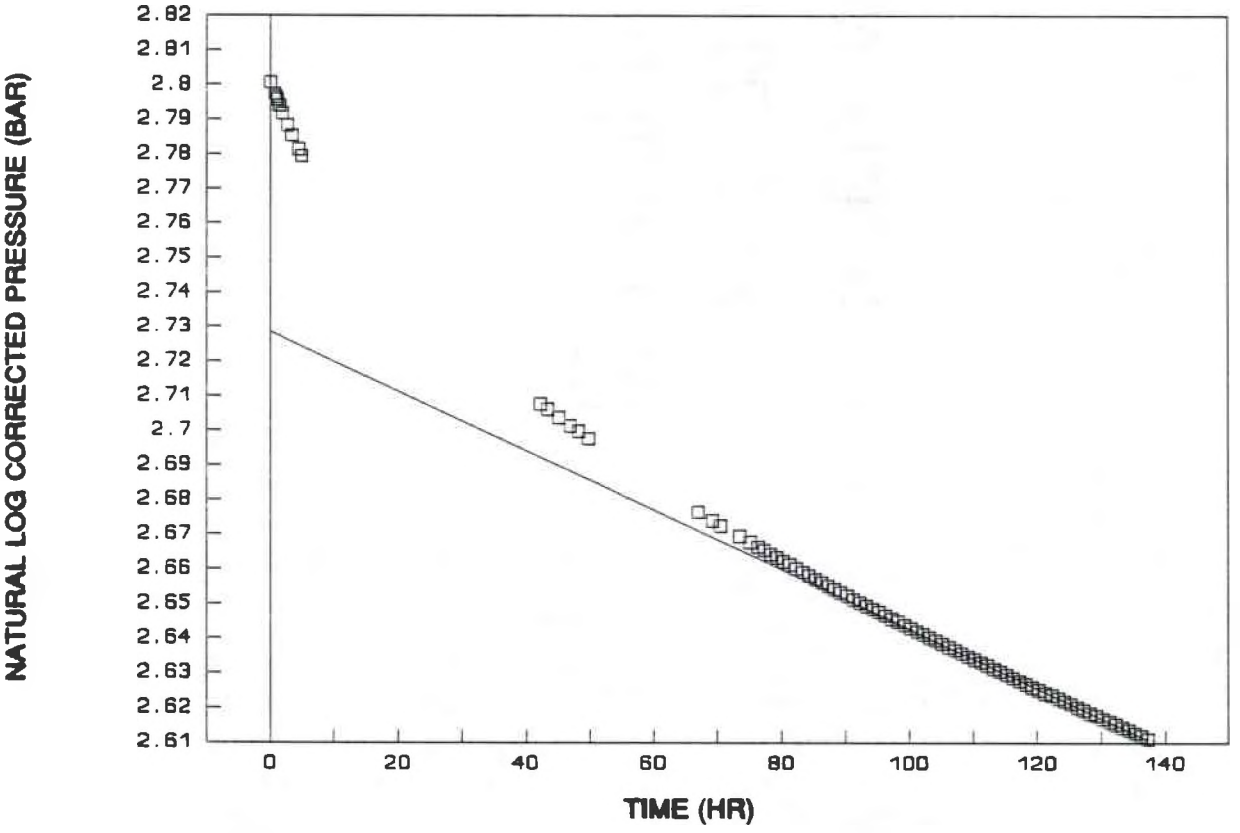

Figure 24. First Order Kinetics at 30°C for Initial 76% Full Charge.

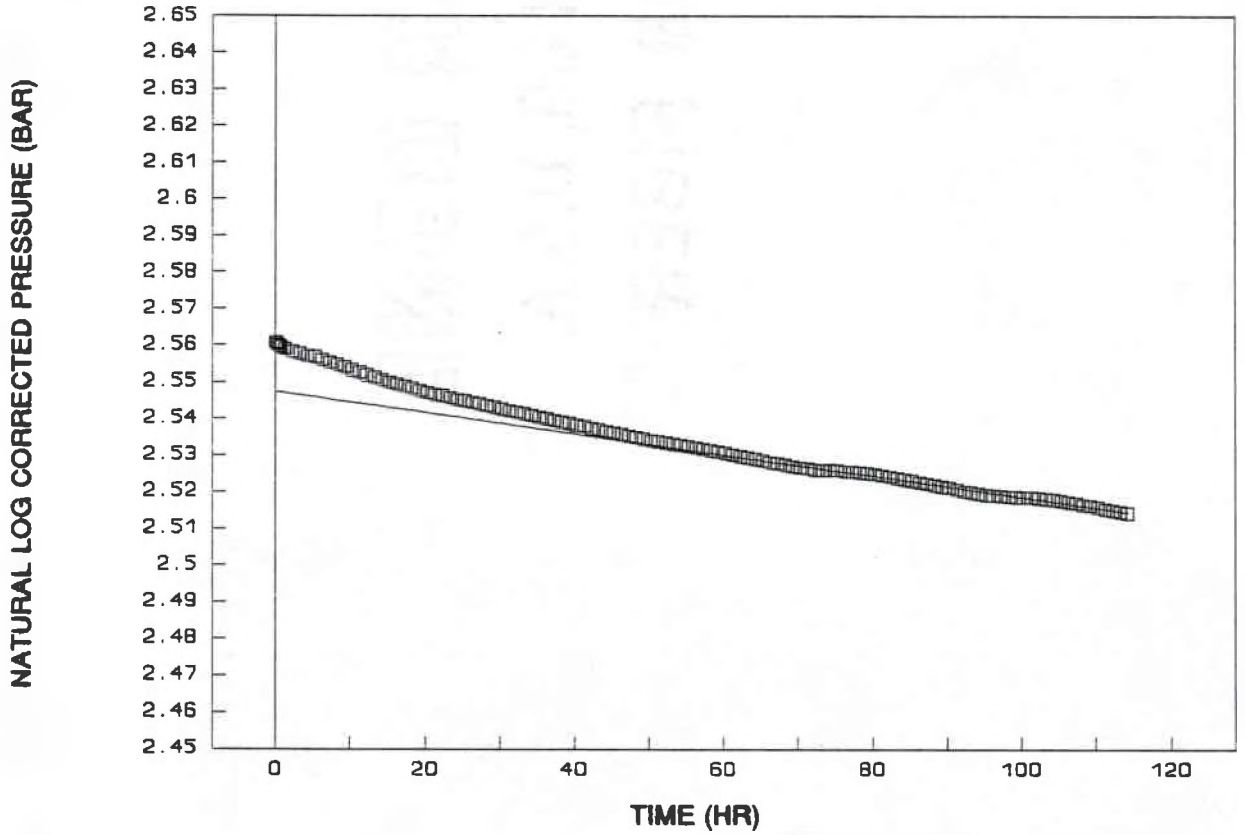

Figure 25. First Order Kinetics at 13°C for Initial 53% Full Charge.

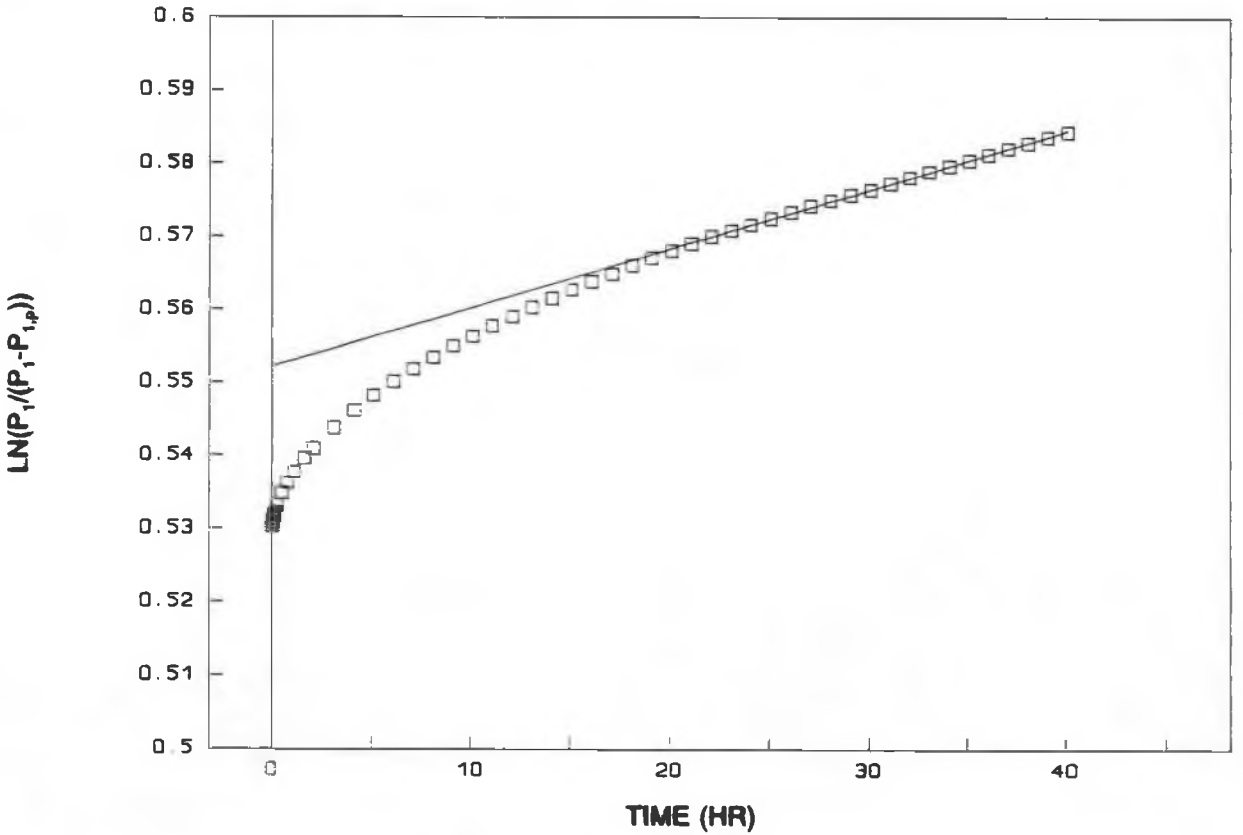

Figure 26. Second Order Kinetics at 11°C.

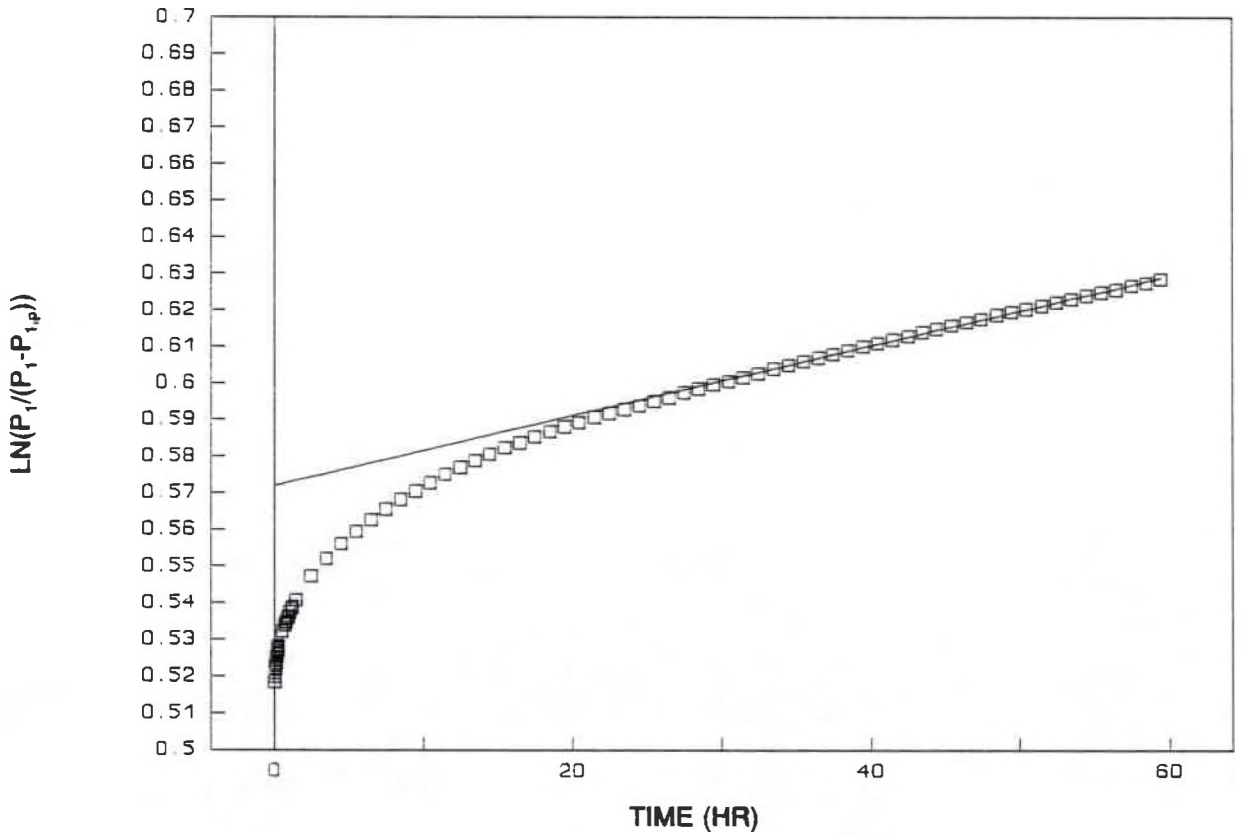

Figure 27. Second Order Kinetics at 21°C.

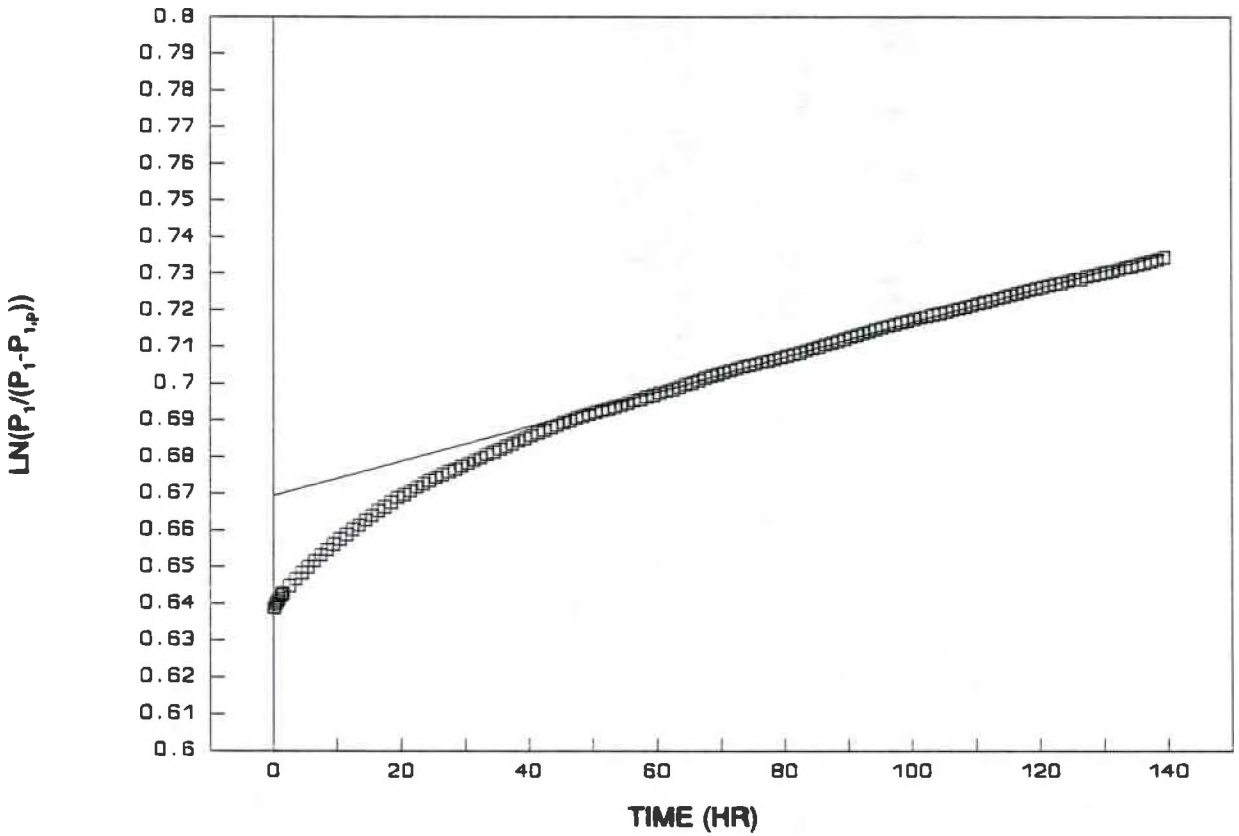

Figure 28. Second Order Kinetics at 11°C for Initial 81% Full Charge.

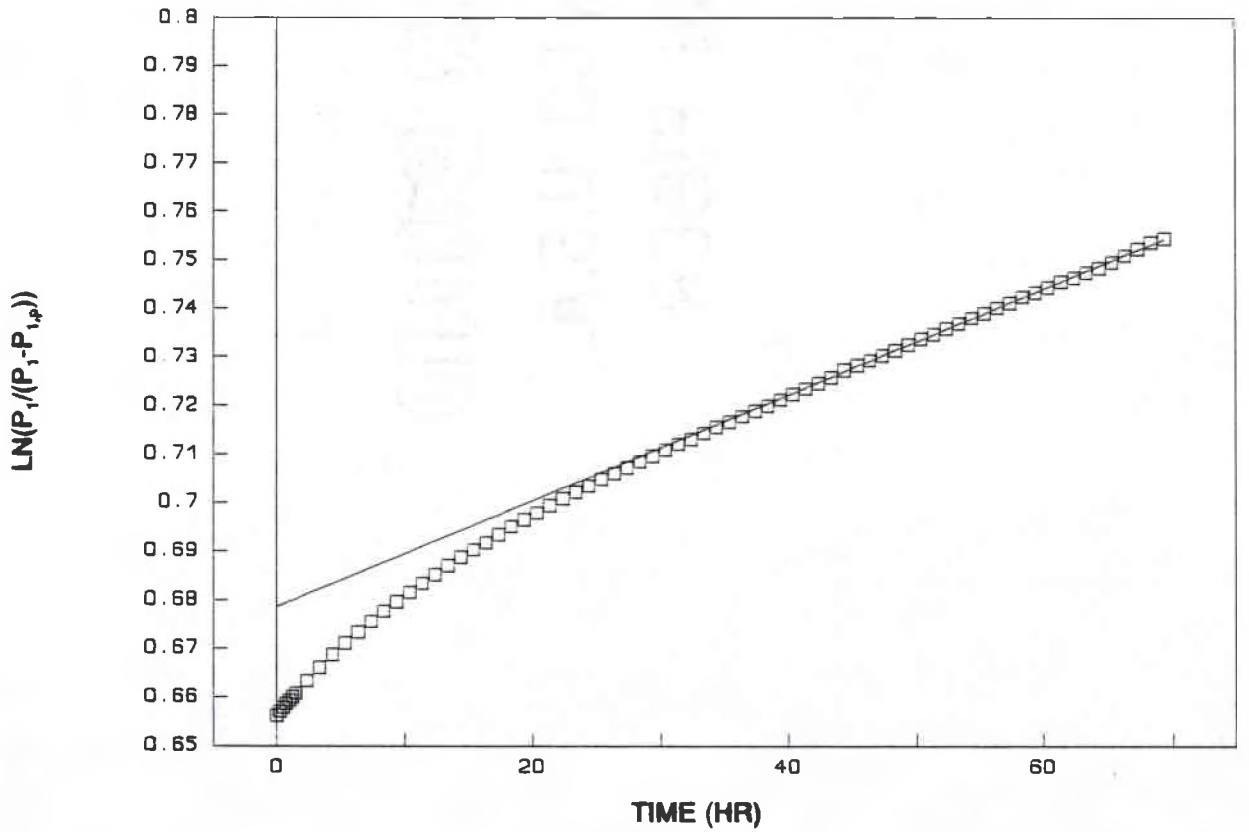

Figure 29. Second Order Kinetics at 21°C for Initial 78% Full Charge.

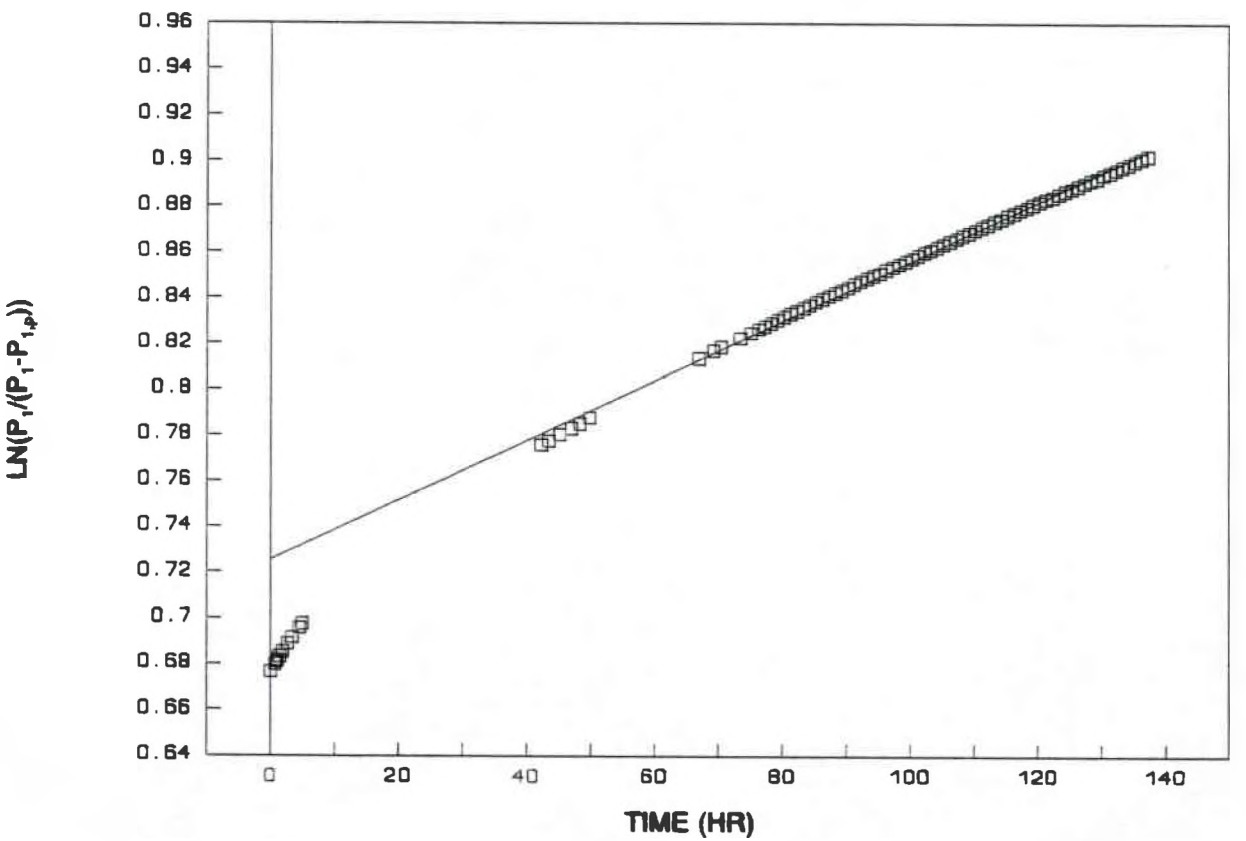

Figure 30. Second Order Kinetics at 30°C for Initial 76% Full Charge.

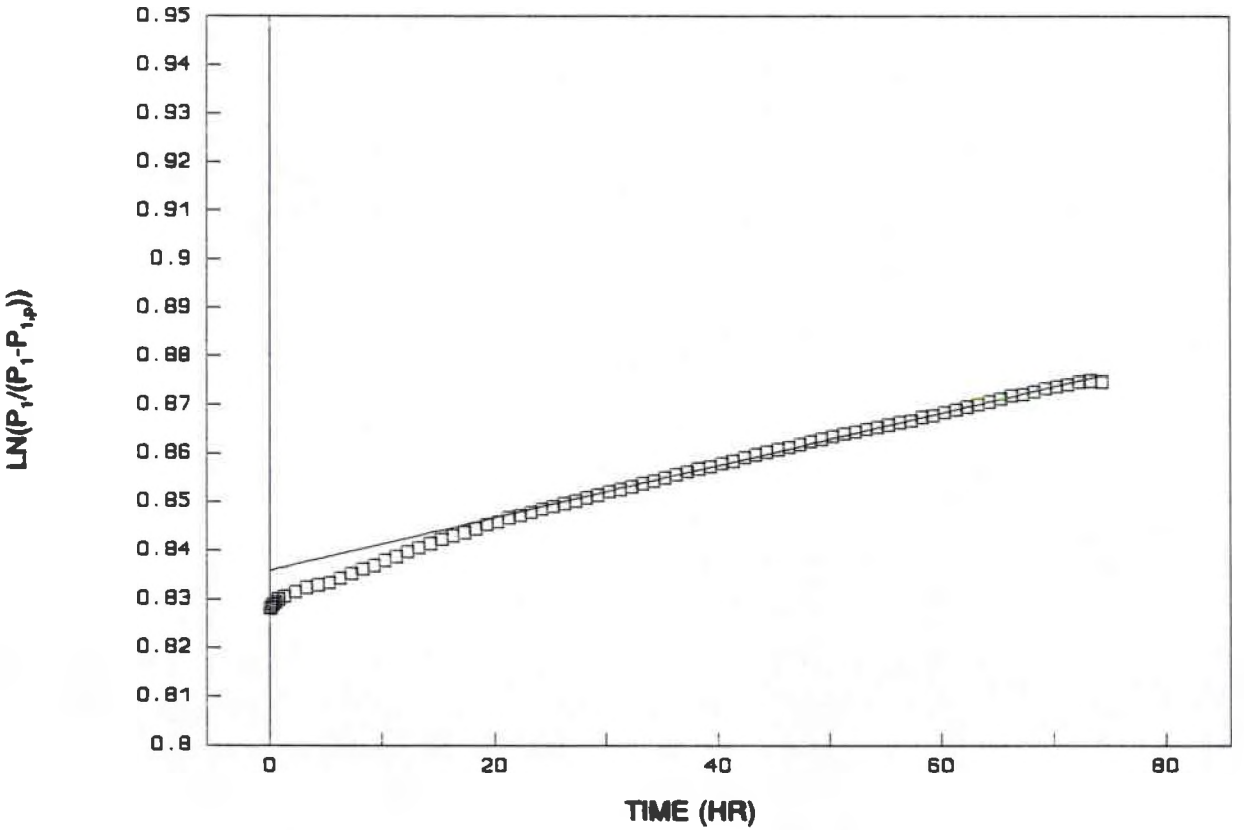

Figure 31. Second Order Kinetics at 13°C for Initial 53% Full Charge.

Any M^2; Numerical Model

The numerical results for M=50 and M=100 are presented in Figs. 32-33. The dimensionless time used in these two figures is defined by the equation shown below.

$$t^* = \frac{D_e}{\varepsilon L_a^2} t \tag{6.1}$$

For M=∞, the reaction rate is diffusion-limited and therefore battery pressure on open-circuit would be described by Eq. (3.20). As M decreases, the influence of kinetic limitations will be seen at short open-circuit times where the self-discharge rate is the highest. Thus, for M=50 (Fig. 32) the transition to a diffusion-limited reaction rate occurs at a t* of about 200 and for M=100 (Fig. 33), this transition takes place at a dimensionless time of about 40.

Therefore, as the Thiele Modulus is decreased, the open-circuit time required for transition to a diffusion-limited reaction increases. This is qualitatively observed in Figs. 14-19. However, further work is required to establish experimental repeatability to insure that the observed effects are indeed solely due to a changing Thiele Modulus.

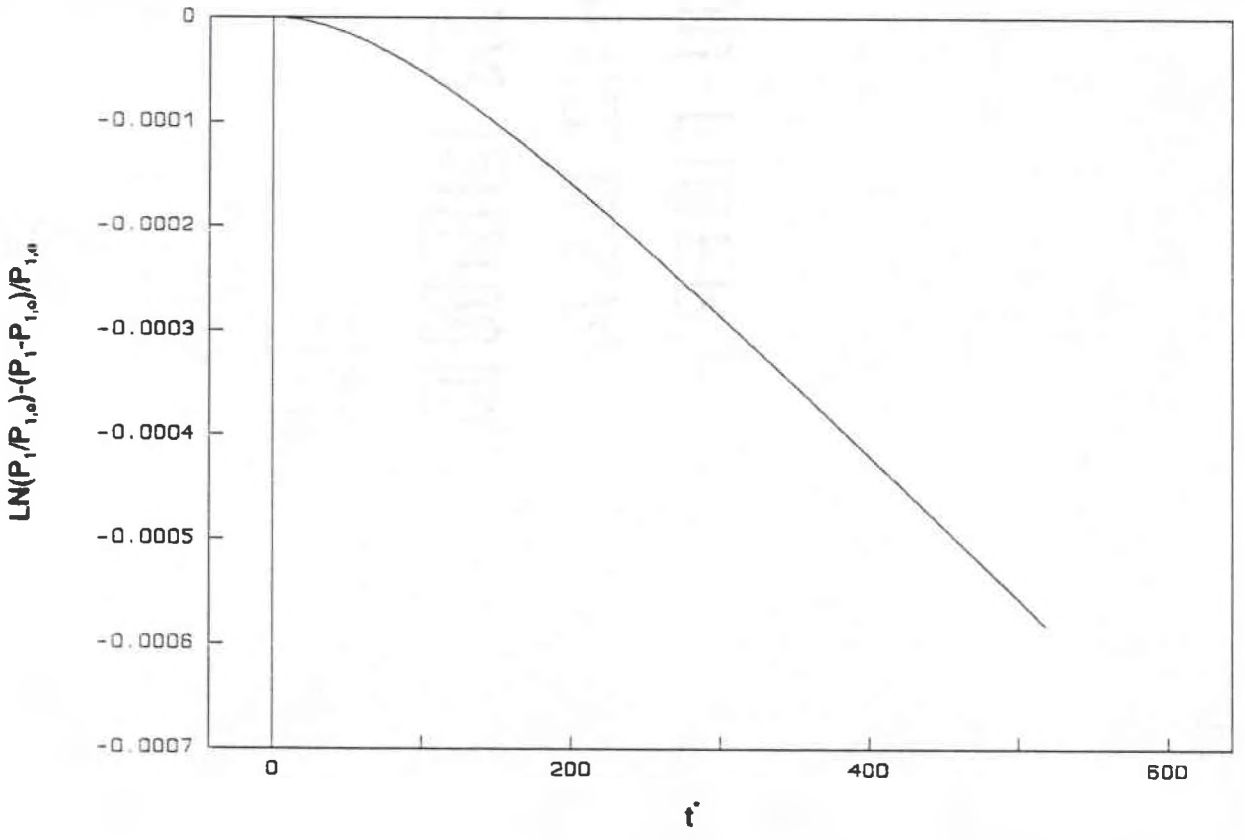

Figure 32. Numerical Simulation for Second Order and M=50.

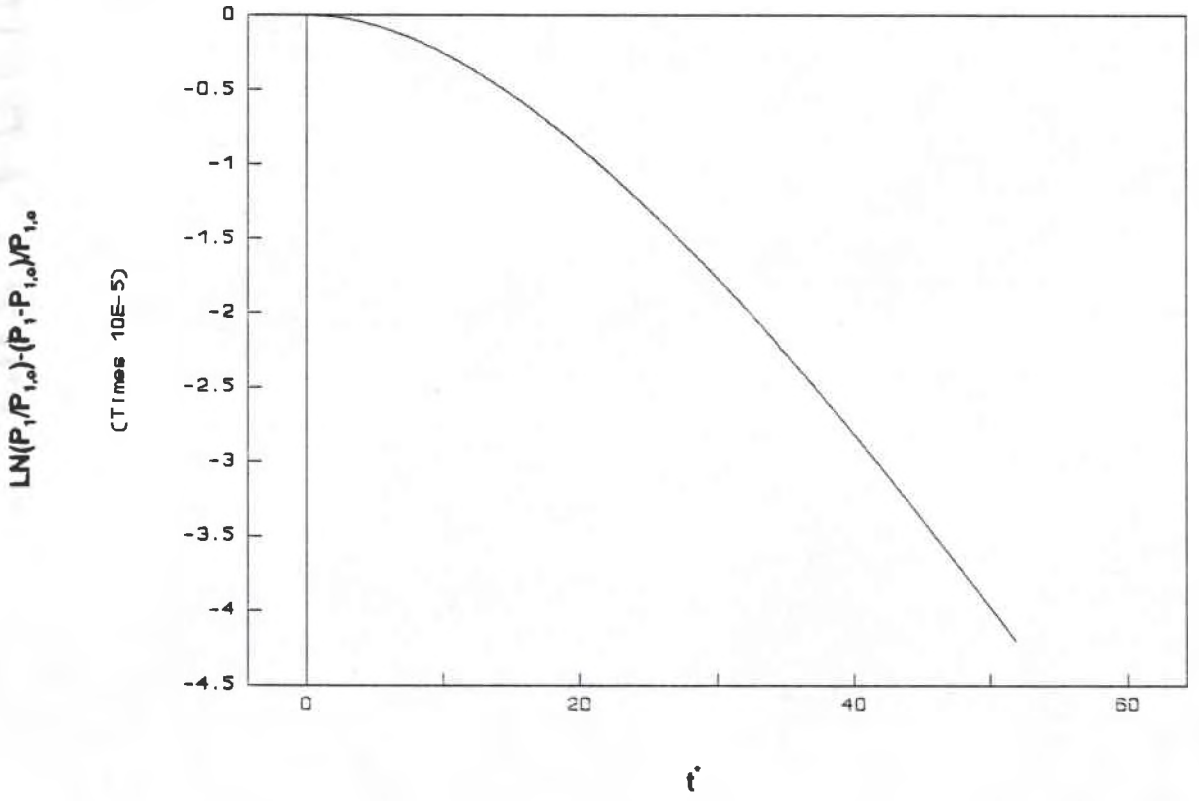

Figure 33. Numerical Simulation for Second Order and M=100.

CHAPTER VII

SUMMARY AND CONCLUSIONS

The purpose of this research was to develop a mass transfer and reaction model of the self-discharge of a nickel-hydrogen electrochemical cell and to verify the resulting model in relation to actual experimental data. Previous proposed models assumed that the kinetics of hydrogen reacting with β-NiOOH limited the rate of the self-discharge reaction. However, the experimental data does not fit the kinetic models at short times and to assume the presence of oxygen to account for this deviation at partial charged conditions is not in accord with experimental evidence. The diffusion with reaction model, however, shows good agreement with the experimental data. At full charge conditions, the open-circuit behavior exhibits diffusion-limited reaction rate behavior. At partial charge conditions, the Thiele Modulus (M) is reduced and the self-discharge behavior first exhibits kinetically limited reaction rate behavior which, with time, shifts to diffusion-limited reaction rate behavior.

Appendix

Crank-Nicolson Implicit Finite Difference Program: Second Order Kinetics with Diffusion

```
      DOUBLE PRECISION LAMDA,DELTAX,C(201),A(201),B(201),CC(201),
     1 D(201),GAMMA(201),ALPHA(201),CONV,DELTAZ,ALP,REA,TA,
     2 TB,TC,RATE,HELP,EFFD,E(201),LE,DE,TM,T,BP,BPP,VB,VBP,VC,
     3 VCP,ZZ,CDISO,BVOL,NHO,NHP
      INTEGER P
      WRITE (*,001)
C
C  FORMAT STATEMENTS
C
  001 FORMAT(1X,'H2 DIFFUSION INTO SOLID WITH RXN PROGRAM; 2ND ORDER
     1  KINETICS')
  102 FORMAT(D12.7)
  103 FORMAT (I8)
  104 FORMAT(1X, 'PLEASE INPUT EFFECTIVE DIFFUSION COEFFICIENT OF H2
     1  DIVIDED BY POROSITY IN CM^V2^V/SEC ')
  105 FORMAT(D12.7)
  106 FORMAT(1X,'EFFECTIVE DIFFUSION COEFFICIENT = ',D12.7)
  200 FORMAT(1X,'PLEASE INPUT NUMBER OF X POINTS')
  300 FORMAT(1X,'DELTAX = ',D12.7)
  350 FORMAT(1X,'PLEASE INPUT NUMBER OF Z POINTS')
  400 FORMAT(1X,'DELTAZ = ',D12.7,5X,'THE NO. OF X POINTS =',I8)
  410 FORMAT(1X,'THE NUMBER OF Z POINTS = ',I8)
  411 FORMAT(1X,'PLEASE INPUT DIFFUSION LENGTH IN CM')
  412 FORMAT (1X,'DIFFUSION LENGTH = ',D12.7)
  413 FORMAT (1X,'PLEASE INPUT BATTERY TEMPERATURE IN
     1  DEGREES K')
  414 FORMAT (1X,'BATTERY TEMPERATURE =',D12.7,'K')
  415 FORMAT (1X,'PLEASE INPUT INITIAL BATTERY PRESSURE,
     1 PSIA')
  416 FORMAT (1X,'BATTERY INITIAL PRESSURE =',D12.7,'PSIA')
  417 FORMAT (1X,'PLEASE INPUT BATTERY PRECHARGE PRESSURE')
  418 FORMAT (1X, 'BATTERY PRECHARGE PRESSURE =',D12.7,
     1 'PSIA')
  419 FORMAT (1X,'COMPRESSIBILITY FACTOR =',D12.7)
  420 FORMAT (1X,'BATTERY GAS VOLUME IN LITERS =')
  421 FORMAT (1X,'BATTERY GAS VOLUME IN LITERS =',D12.7)
  640 FORMAT (1X,'Z = ',F12.7)
  650 FORMAT (1X,F12.7,10X,F12.7,10X,F12.7)
  750 FORMAT (1X,F12.7)
```

```
  991 FORMAT(1X,'THIELE MODULUS M =')
  992 FORMAT(D12.7)
  993 FORMAT(1X,'M =',D12.7)
C
C  INPUT STATEMENTS
C
C  VALUE OF THE NUMBER OF X-POINTS (INCLUDING THE ENDS) IS K
      WRITE (*,200)
      READ (*,103) K
C  VALUE OF THE NUMBER OF TIME Z-POINTS (INCLUDING THE ENDS)
C  IS NN; ONE DAY BASIS
      WRITE (*,350)
      READ (*,103) NN
C  VALUE OF EFFECTIVE DIFFUSION COEFFICIENT OF HYDROGEN/POROSITY
C    IS DE  (UNITS CONVERTED FROM INPUT CM2/SEC TO CM2/DAY)
      WRITE (*,104)
      READ (*,105) DE
      WRITE (*,106) DE
      DE = DE*3600*24
C  VALUE OF ACTIVE MATERIAL LENGTH IS LE (UNIT IS CM)
      WRITE (*,411)
      READ (*,105) LE
      WRITE (*,412) LE
C  VALUE OF THIELE MODULUS IS TM (DIMENSIONLESS)
      WRITE (*,991)
      READ (*,992) TM
      WRITE (*,993) TM
C  VALUE OF BATTERY TEMPERATURE IS T (UNIT IS KELVIN)
      WRITE (*,413)
      READ (*,105) T
      WRITE (*,414) T
C  VALUE OF INITIAL AND PRECHARGE BATTERY PRESSURE ARE BP AND BPP,
C    RESPECTIVELY (UNITS ARE PSIA)
      WRITE (*,415)
      READ (*,105) BP
      WRITE (*,416) BP
      WRITE (*,417)
      READ (*,105) BPP
      WRITE (*,418) BPP
C  VALUE OF BATTERY GAS VOLUME IS BVOL (UNITS ARE LITERS)
      WRITE (*, 420)
      READ (*,105) BVOL
      WRITE (*,421) BVOL
C
C  INITIAL CALCULATIONS
C
C  VALUE OF DIMENSIONLESS DISTANCE STEPSIZE IS DELTAX
      DELTAX = (1.)/ (FLOAT(K)-1.)
      WRITE (*,300) DELTAX
C  VALUE OF TIME STEPSIZE IS DELTAZ (UNIT IS DAY)
      DELTAZ = (1.)/(FLOAT(NN)-1.)
```

```
C  VALUE OF DELTAZ/(DELTAX**2) IS LAMDA (UNIT IS DAY)
      LAMDA = DELTAZ/((DELTAX)**2)
      WRITE (*,400) DELTAZ,K
      WRITE (*,410) NN
C  VALUE OF DIFFUSIVITY/(POROSITY*LENGTH**2) IS ALP (UNIT IS 1/DAY)
      ALP = DE/(LE**2)
C  VALUE OF KINETIC RATE CONSTANT/POROSITY IS RATE
C    (UNIT IS (CM**3)/(GMOL*DAY)
      RATE = (TM**2)*DE/((LE**2)*0.042)
C  CALCULATE VIRIAL COEFFICIENTS AND INITIAL
C  COMPRESSIBILITY FACTOR ZZ
C    (NOTE:  VIRIAL COEFFICIENT DATA FOR HYDROGEN TAKEN
C     FROM LEROY, R, ET.AL., "THE THERMODYNAMICS OF AQUEOUS
C     WATER ELECTROLYSIS," JOURNAL OF THE ELECTROCHEMICAL
C     SOCIETY, VOL. 127, NO. 9, (1980), P. 1954.
      VB = 20.5 - 1857./T
      VBP = VB/(82.05*T)
      VC = -351.+12760./(T**(.5))
      VCP = (VC - (VB)**2)/((82.05*T)**2)
      ZZ = 1. + VBP*(BP/14.696)+VCP*((BP/14.696)**2)
      WRITE (*,419) ZZ
C  CALCULATE INITIAL DISSOLVED HYDROGEN CONCENTRATION CDISO (BASED ON
C  HENRY'S LAW, 7M KOH AND 21C, DATA FROM KNASTER, M. AND APEL'BAUM, L.,
C  "SOLUBILITY OF HYDROGEN AND OXYGEN IN CONCENTRATED POTASSIUM
C  HYDROXIDE SOLUTION," RUSSIAN JOURNAL OF PHYSICAL CHEMISTRY, VOL. 38,
C  NO. 1, (1964), P. 120.                    UNIT IS GMOL/CM**3)
      CDISO = BP/(14.696*8918725.)
C  CALCULATE INITIAL TOTAL AND PRECHARGE MOLES OF HYDROGEN, NHO AND
C    NHP, RESPECTIVELY (UNITS ARE GRAM-MOLES)
      NHO = (BP/14.696)*(BVOL)/(0.082*T*ZZ)
      ZZ = 1. + VBP*(BPP/14.696)+VCP*((BPP/14.696)**2)
      NHP = (BPP/14.696)*(BVOL)/(0.082*T*ZZ)
C
C  SET THE INITIAL CONDITIONS
C
C   FULL CHARGE CONDITION; NO HYDROGEN IN ELECTROLYTE/ACTIVE MATERIAL
C   EXCEPT AT INTERFACE BETWEEN GAS FILLED MACROPORES AND ELECTROLYTE/
C   ACTIVE MATERIAL
      DO 600 I = 1,K
      E(I) = .042
  600 C(I) = 0.
      P = (K-1)/2
      DO 588 I = 1,P
      C(I) = 0.
  588 E(I) = .042
      M = 0
      Z = 0.
      C(1) = 1.
C
C  OPEN FILE 'OUT' FOR STORAGE OF DATA
C
```

```
      OPEN (7,FILE='OUT',STATUS='OLD',ACCESS='SEQUENTIAL')
C
C  BODY OF THE PROGRAM
C
  009 Z = (FLOAT(M))/(FLOAT(NN-1))
C
C  AT CERTAIN VALUES OF Z, THE CONCENTRATION VALUES AND THE AMOUNT OF
C  NICKEL OXYHYDROXIDE REACTED ARE SAVED.  THE PROGRAM IS TERMINATED
C  AFTER ONE DAY OF SIMULATION (Z = 1.0.).
C
      IF (Z.EQ.(0.1)) GOTO 5
      IF (Z.EQ.(0.2)) GOTO 5
      IF (Z.EQ.(0.3)) GOTO 5
      IF (Z.EQ.(0.4)) GOTO 5
      IF (Z.EQ.(0.5)) GOTO 5
      IF (Z.EQ.(0.6)) GOTO 5
      IF (Z.EQ.(0.7)) GOTO 5
      IF (Z.EQ.(0.8)) GOTO 5
      IF (Z.EQ.(0.9)) GOTO 5
      IF (Z.EQ.(1)) GOTO 5
  012 IF (Z.GE.(1)) GOTO 999
      M = M + 1
C
C  START OF THOMAS ALGORITHM TO CALCULATE THE CONCENTRATIONS
C
C  THE ALPHA AND GAMMA VALUES AT I = 2
C
      N = K-1
      ALPHA(2) = ((-1.)/2.*LAMDA*ALP)/(1+LAMDA*ALP)
      GAMMA(2) = (C(2)-DELTAZ*RATE*(C(2))*(E(2))+
     1   (1./2.)*ALP*LAMDA*(2.*(C(1))-2.*(C(2))+C(3)))/(1.+
     2    LAMDA*ALP)
C
C  A(I), B(I), CC(I) AND D(I) VALUES AT I = 3 TO N (OR K-1)
C
      DO 601 I = 3,N
      A(I) = (-1.)/2.*LAMDA*ALP
      B(I) = LAMDA*ALP+1.
      CC(I) = (-1.)/2.*LAMDA*ALP
  601 D(I) = (C(I) - DELTAZ*RATE*(C(I))*(E(I)) +
     1    (1./2.)*ALP*LAMDA*(C((I-1))-2.*(C(I))+C((I+1))))
C
C  CC(N), B(N) AND D(N) VALUES
C
      CC(N) = 0
      B(N) = 1. + ALP*LAMDA/2.
      D(N) = (C(N) - DELTAZ*RATE*(C(N))*(E(N)) +
     1    (1./2.)*ALP*LAMDA*(C((N-1)) - C(N)))
C
C  ALPHA(I) AND GAMMA(I) VALUES AT I = 3 TO N (OR K-1)
C
```

```
      DO 602 I = 3,N
      ALPHA(I) = CC(I)/(B(I)-A(I)*ALPHA((I-1)))
  602 GAMMA(I) = (D(I)-A(I)*GAMMA((I-1)))/(B(I)-A(I)*ALPHA((I-1)))
C
C  CONCENTRATION VALUES AT K AND K-1
C
      C(N) = GAMMA(N)
      C(K) = C(N)
C
C  CONCENTRATION VALUES AT I = K-2 TO 2
C
      J = N - 1
      DO 603 I = 2,J
      L = K - I
  603 C(L) = GAMMA(L) - ALPHA(L)*C((L+1))
C
C  BALANCE ON NIOOH
C
      DO 605 I = 1,K
      E(I) = E(I) - 2.*DELTAZ*RATE*(C(I))*(E(I))*CDISO
 605  IF ((E(I)).LE.0)E(I) = 0.
C
C  END OF THE THOMAS ALGORITHM
C
C  CALCULATING THE FRACTIONAL CONVERSION OF NIOOH, CONV, BY THE SIMPSON
C    INTEGRAL METHOD
C
      TA = 0.
      TB = 0.
      TC = 0.
      REA = 0.
      DO 850 I = 2,(K-1),2
  850 TA = TA + 4*E(I)
      DO 855 I = 3,(K-2),2
  855 TB = TB + 2*E(I)
      TC = E(1) + E(K)
      REA = DELTAX/3*(TA+TB+TC)
      CONV = (0.042-REA)/(0.042)
C
C  CALCULATE NEW BATTERY PRESSURE, BPP (PSIA), AND NEW SURFACE DISSOLVED
C    HYDROGEN CONCENTRATION, C(1) (DIMENSIONLESS).
C
      ZZ = 1. + VBP*(BP/14.696)+VCP*((BP/14.696)**2)
      BP = 14.696*(.082)*ZZ*T*(NHP+(NHO-NHP)*(1.-CONV))/BVOL
      C(1) = BP/(CDISO*14.696*8918725.)
C
C  DO THE SAME CALULATIONS AGAIN FOR THE NEXT Z - INCREMENT
C
      GOTO 9
C
C
```

```
C  PRINT THE VALUES TO THE SCREEN AND FILE
C
C
C
  005 WRITE (*,640) Z
      WRITE (7,640) Z
      DO 700 I = 1,K
      XX = (FLOAT(I)-1)/(FLOAT(K)-1)
      WRITE (7,650) XX,C(I),E(I)
  700 WRITE (*,650) XX,C(I),E(I)
C
C  PRINTING THE FRACTIONAL CONVERSION OF NIOOH TO BOTH SCREEN AND FILE
C
      WRITE (*,750) CONV
      WRITE (7,750) CONV
C
C  RETURN
C
      GOTO 12
C
C  END OF PROGRAM
C
  999 CLOSE (7)
      STOP
      END
```

REFERENCES

1. Font, S. and Goualard, J., "Ni-H_2 Performance versus Ni-Cd," Power Sources 5, ed. by Collins, D. H., Academic Press, New York, (1975), p. 331.

2. McBreen, J., "The Nickel Oxide Electrode," Modern Aspects of Electrochemistry, ed. by White, R. E. et. al., No. 21, Plenum Press, New York, (1990), p. 29.

3. Buder, B., "Oxygen Evolution during Recharging of Positive Nickel Oxide Sinter Electrodes," Journal of Applied Electrochemistry, Vol. 2, (1972), p. 301.

4. Warnock, D., "Design of Nickel-Hydrogen Cells for Spacecraft," Proceedings of the Symposium on Battery Design and Optimization, ed. by Gross, S., PV 79-1, The Electrochemical Society, Inc., (1979), p. 163.

5. Visintin, A., et. al., "Microcalorimetry Study of Ni/H_2 Battery Self-Discharge Mechanism," Proceedings of the 6th Annual Battery Conference on Applications and Advances, California State University, Long Beach, CA, (1991).

6. Greaves, C. and Thomas, M. A., "Refinement of the Structure of Deuterated Nickel Hydroxide, ($Ni(OD)_2$), by Powder Neutron Diffraction and Evidence for Structural Disorder in Samples with High Surface Area," Acta Cryst. B42, (1986), p. 51.

7. Barnard, R., et. al., "Studies Concerning Charge Nickel Hydroxide Electrodes. I. Measurement of Reversible Potentials," Journal of Applied Electrochemistry, Vol. 10, (1980), p. 109.

8. Bratsch, S., "Standard Electrode Potentials and Temperature Coefficients in Water at 298.15 K," J. Phy. Chem. Ref. Data, Vol. 18, No. 1, (1989), p. 1.

9. Holleck, G., "Self-Discharge of Nickel-Hydrogen Cells," Proceedings of the 1977 Goddard Space Flight Center Battery Workshop, NASA CP-2041, (1977), p. 525.

10. Stockel, J. F., "Self-Discharge Performance and Effects of Electrolyte Concentration on Capacity of Nickel-Hydrogen (Ni-H_2) Cells," 20th Intersociety Energy Conversion Engineering Conference, (1985), p. 1.171.

11. Ritterman, P. F. and King, A. M., "The Open-Circuit Stand Behavior Intelsat VI Nickel Hydrogen Batteries and its Relationship to Charge Rates and Temperature," 20th Intersociety Energy Conversion Engineering Conference, (1985), p. 1.175.

12. Kim, Y. J., Visintin, A., Srinivasan, S., and Appleby, A. J., "Microcalorimetric Study on Self-Discharge of Nickel Hydroxide Electrodes," Proceedings of the Symposium on Nickel Hydroxide Electrodes, PV 90-4, The Electrochemical Society, Inc., (1990), p. 368.

13. Mao, Z., Visintin, A., Srinivasan, S., and Appleby, A. J., "Microcalorimetric Study of Self-Discharge Mechanism of Ni-H2 Batteries," Abstract No. 11, Extended Abstracts, Vol. 91-1, Electrochemical Society, (1991), p. 15.

14. Zhang, C., et. al., "Hydrogen Oxidation on Nickel Electrodes in Alkaline Media," Proceedings of the Symposium on Nickel Hydroxide Electrodes, PV 90-4, The Electrochemical Society, Inc., (1990), p. 356.

15. Tsenter, B. I. and Sluzhevskii, A. I., "Kinetics of Self-Discharge of a Sealed Nickel-Hydrogen Battery," Zhurnal Prikladnoi Khimii, Vol 54, No. 11, (1981), p. 2545.

16. Abbey, K. M. and Thaller, L. H., Pore Size Engineering Applied to Starved Electrochemical Cells and Batteries, NASA-TM-82893, (1982).

17. Crank, J., The Mathematics of Diffusion, Oxford University Press, New York, (1975).

18. Wen, C., "Noncatalytic Heterogeneous Solid Fluid Reaction Models," Industrial and Engineering Chemistry, Vol. 60, No. 9, (1968), p. 34.